Structured Packings for Multiphase Catalytic Reactors

ARTICLE *in* INDUSTRIAL & ENGINEERING CHEMISTRY RESEARCH · APRIL 2008

Impact Factor: 2.59 · DOI: 10.1021/ie800067r

REVIEWS

Structured Packings for Multiphase Catalytic Reactors

Kalyani Pangarkar,*,†,§ Tilman J. Schildhauer,‡ J. Ruud van Ommen,§ John Nijenhuis,§ Freek Kapteijn,*,† and Jacob A. Moulijn†

Catalysis Engineering, Delft University of Technology, Julianalaan 136, 2628 BL, Delft, The Netherlands, Laboratory for Energy and Materials Cycles, Paul Scherrer Institut, 5232 Villigen PSI, Switzerland, and Product and Process Engineering, Delft University of Technology, Julianalaan 136, 2628 BL, Delft, The Netherlands

Reactor design for multiphase catalytic fixed bed reactors is always based on conflicting objectives. In the past, catalyst discovery and development preceded and motivated the selection of an appropriate multiphase reactor type. This type of sequential approach is increasingly been replaced by a parallel approach to catalyst and reactor selection. In nearly all respects, structured catalysts and reactors have the ability to outperform randomly packed reactors. Structured packings, apart from their advantages of high voidage and low-pressure drop, have the benefit of ease of scale-up and accurate description of the fluid mechanics. In this review we have evaluated the potential of using structured internals for multiphase catalytic reactions, which are currently carried out in randomly packed fixed bed reactors. Characteristics of various structured internals such as monoliths, corrugated sheet or gauze packings, knitted wire packings and foams are discussed in detail. Since designing a structured device for gas−liquid−solid contacting requires a sound knowledge of hydrodynamics and transport phenomena, a concise review of the above-mentioned structured packings and their characteristics based on hydrodynamics and transport phenomena is presented. Existing models (empirical, phenomenological and mechanistic) are outlined with respect to flow regime transition, pressure drop, liquid hold-up, gas−liquid interfacial area, gas to liquid mass transfer, liquid to solid mass transfer, residence time distribution (RTD), and heat transfer. The models are critically evaluated, and their limitations are discussed. An overview is given about what information is available, what needs to be evaluated and what kind of existing methodology can be applied in order to arrive at quantitative models for the physical parameters. Last, the structured internals are compared with each other and with randomly packed bed reactors, allowing a rational selection of the preferred packing for a given application.

1. Current Multiphase Reactors

Multiphase reactors are found in diverse applications such as in manufacture of petroleum-based fuels and products, in production of commodity and specialty chemicals, pharmaceuticals, herbicides and pesticides, in production of materials and in pollution abatement.[1] A key motivation for implementing multiphase reactor technology has largely been driven by the discovery and development of new or improved catalysts for either emerging or existing processes.[2] Typical reaction types that are encountered in multiphase processes of the chemical industry are summarized in Dudukovic et al.[2] A wealth of products are produced in multiphase catalytic reactions. Among the multiphase reaction systems, the stirred tank slurry reactor, slurry bubble column and the trickle bed reactor are being used most extensively. The pros and cons of the various reactor types are summarized in Table 1.

It is evident from the information given in the table that an optimum has still not been reached with respect to reliable reactor performance. Every type has its pros and cons. While bubble columns and stirred tank reactors have the advantage of small catalyst particles, trickle bed reactors do not have any problems associated with catalyst separation. The major disadvantage of the stirred tank and slurry bubble column reactors is the required separation of product and catalyst, necessitating a filtration step of the fine catalyst particles from the liquid product. Moreover, when applied in the continuous mode, back mixing lowers the conversion and usually the selectivity. A packed bed reactor, such as the trickle bed reactor, is much more convenient but large particles (>1 mm) have to be used to limit the pressure drop. A summary of the most important processes carried out in trickle-bed reactors is given in Al-Dahhan et al.[3] Trickle bed reactors are typically applied for processes involving slow reactions because of their advantage of high catalyst loading and longer residence time and its narrower distribution. Because of the low and tortuous porosity of the packed bed, liquid flow rates are limited to low values in order to avoid the development of pockets of stagnant liquid, which can lead to an undesired high-pressure drop and eventually flooding, when in countercurrent operation. Flooding occurs at high gas and high liquid flow rates and is characterized by accumulation of liquid across the bed cross-section disabling further operation. Therefore, due to the limitations imposed on the flow rates, packed beds show incomplete catalyst wetting and poor mass transfer rates and are nearly always used in the co-current mode. In view of the rapid improvements in the area of catalysis, leading to highly active catalyst particles, severe intraparticle diffusion and heat transport limitations can be foreseen in these reactors. Thus, difficulties with heat removal may lead to hot

* To whom correspondnece should be addressed. Fax: +31-15-2785006. E-mail addresses: kalyanimv@hotmail.com, f.kapteijn@tudelft.nl.

† Catalysis Engineering, Delft University of Technology.

‡ Laboratory for Energy and Materials Cycles, Paul Scherrer Institut.

§ Product and Process Engineering, Delft University of Technology.

10.1021/ie800067r CCC: $40.75
Published on Web 05/01/2008

Table 1. Qualitative Comparison of Existing Multiphase Catalytic Reactors[a]

aspects considered		stirred tank slurry reactor	slurry bubble column	trickle bed reactor
reactor	type	mixed	plug flow/ mixed	dispersed plug flow
catalyst	separation	difficult	difficult	simple
	replacement	simple	simple	difficult
	manufacture	established	established	established
	loading	low−moderate	low−moderate	high−low pure catalyst−egg shell catalyst
	utilization	high	high	low−moderate
mass transfer	internal	good	good	bad-good
	liquid−solid	good particles in suspension small particles	good particles in suspension small particles	fair particles stationary larger particles
	gas−liquid	moderate larger bubble size	moderate larger bubble size	fair sufficient gas−liquid interaction
RTD	gas and liquid	backmixing for both gas and liquid	backmixing for liquid and small bubbles	axially dispersed plug flow for both gas and liquid
heat transport	to outside	very good	very good	low-moderate
scale-up	hydrodynamics	difficult	difficult	medium
	high pressure	costly	fair	fair

[a] Data taken from ref 4.

spots resulting in catalyst deactivation. The heat removal problem is also one of the main causes for lower selectivity toward the desired product in many processes. It is self-evident that these limitations are unfavorable from the point of view of process economics. This motivates a systematic research for alternative reactor types that will overcome as much as possible the limitations in the existing reactors.

2. Structured Internals for Multiphase Catalytic Reactors

Process intensification draws a lot of attention and it has become clear that multifunctional and structured reactors will play a key role in the near future.[5] A structured reactor contains a structured internal which can be made out of ceramics, metals or carbon, situated inside a reactor. It can be considered as an intensified form of a randomly packed bed reactor. A monolith is an example of a structured reactor; in fact, the borderline between catalyst and reactor vanishes for this application.[6]

The advantage of a structured reactor is that it may be designed in full detail up to the local surroundings of the catalyst, allowing ultimate precision.[7] The exact shape and size of all column internals is determined by design rather than chance.[7] Moreover, these structured reactors show flexibility with respect to different length scales, i.e., diffusion lengths, voidage etc. They effectively allow the decoupling of intrinsic reaction kinetics, transport phenomena and hydrodynamics.[8] This decoupling is extremely valuable because it allows independent optimization for all these three aspects, each of which has a significant influence on the behavior of a catalytic reactor, giving rise to a reliable and excellent reactor performance.[8] The best example where decoupling between hydrodynamics and reaction rates is needed is the requirement of small particles for high catalyst effectiveness whereas hydrodynamics is demanding a low-pressure drop, and as a consequence, the particles should be large. These two are the classical conflicting demands in a packed bed. In such cases structured internals can play a very important role and allow solutions that were previously impossible. Structured internals such as monoliths can be coated with catalysts, supports or their precursors.[5] Due to the short diffusion distances obtained by coating, the catalytically active material can be utilized more efficiently.

Usually structured internals do have disadvantages, the major ones being low catalyst loading, when the catalyst is present as a coating, and high costs. To achieve comparable catalyst loadings with that of a randomly packed bed, either a high geometric area of the structured internal or an integral structured catalyst is a prerequisite. If the catalyst is coated on the surface of the structured internal, then the stability and resistance of the coating to adverse conditions such as high pressure and temperature need to be considered.

Adequate knowledge of the hydrodynamics and transport parameters is a key to designing an efficient structured catalytic reactor. For a good design, the hydrodynamics and transport processes need to be described in satisfactory way.[4] A catalytic reactor can never perform better than the catalyst and, as a consequence, catalyst preparation methodology should be further developed for various structured internals made of different materials required for specific applications. Thus, research is needed to provide the enabling tools fully exploiting the high potential of structured reactors.

3. Goal and Structure of the Review

The goal of this review is to provide concise information on the hydrodynamics and transport phenomena based on existing data in different structured packings applicable for multiphase catalytic reactors. This information is then used to bring out a table for a user-friendly rational selection of randomly packed bed and structured multiphase catalytic reactors.

The next two sections discuss the currently envisaged types of structured packings with a focus upon the hydrodynamic and transport parameters.

The sections 6.1−6.5 focus in more detail on monoliths, corrugated open crossflow packings, corrugated closed crossflow packings, knitted packings, and foams. The correlations for hydrodynamic and transport parameters resulting from these studies are discussed critically.

The last two sections sum up what information is available, what needs to be evaluated and what kind of existing methodology can be applied in order to arrive at quantitative models for the physical parameters. A concise matrix of relevant process parameters with ranking for the individual packings is presented.

4. Structured Internals for Reaction and Separation

Since the 1960s structured packings have been applied successfully in industrial distillation and absorption columns.[9] It is estimated that already 25% of all refinery towers worldwide are fitted with structured packings.[10] The main type of structured packing used in the process industry is the corrugated plate type packing. They are mainly used to create sufficient gas−liquid contact area, which is essential for a good separation. A typical example is the application of corrugated wire gauze packings to purify oleochemicals such as glycerol, fatty acids, and fatty alcohols and wax esters in vacuum distillation.[11] As these

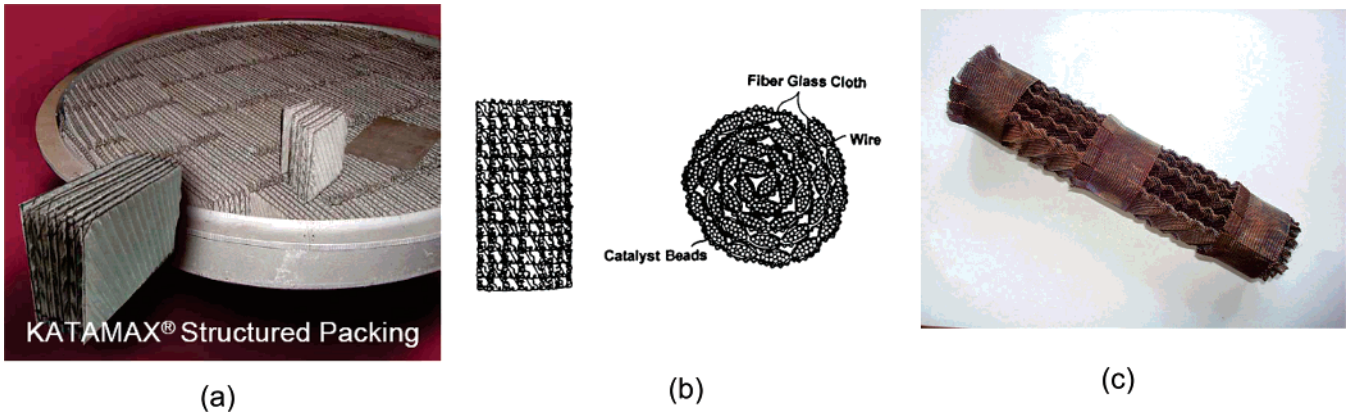

Figure 1. Different types of structured packings (from left to right): (a) Katamax developed by Koch Engineering; (b) catalyst bales developed by CDTech; and (c) Katapak for laboratory-scale tests.[52]

products are extremely heat sensitive, they have to be distilled at low temperatures and therefore vacuum conditions are preferred. The corrugated wire gauze packings are extremely efficient for these applications, as they do not have to operate under a high-pressure drop. The inherent capillary action of the wire gauzes is sufficient to facilitate the liquid spreading on the packing. On the one hand, for trickle bed reactors the use of structured packings is yet hardly commercialized and is still limited to lab scale research. On the other hand, structured packings are in increasing demand for reactive distillation applications where reaction and separation is carried out in one single process.

A number of reactive distillation packing concepts have been developed to fulfill the required criteria, few examples "catalyst bales" developed by CDTech (Catalytic Distillation Technologies), Katapak-S developed by Sulzer ChemTech and Katamax developed by Koch Engineering. Sketches of the packings are presented in Figure 1.

A commercial process illustrating the use of corrugated structured packings is the hydrolysis of methyl acetate using Katapak-SP packing. Sulzer ChemTech has developed this process together with Wacker-Chemie and the first plant is in operation at Wacker's site in Burghausen, Germany, since 2000.[12] In this process, methyl acetate and excess water are fed to a prereactor, where the hydrolysis reaction takes place almost to chemical equilibrium. The reactor outlet product is fed to the reactive distillation column, where reaction conversion is increased up to 97%. By continuously removing the products from the reactive section, a shift of the chemical equilibrium of the hydrolysis reaction can be achieved leading to an increase in overall conversion. A simplified process flow scheme of this process is presented in Figure 2.

Other structured catalysts frequently encountered are ceramic monolithic catalysts.[6] They have found many applications in combustion and environmental uses, e.g., as afterburners of engine exhausts and for removal of harmful compounds from industrial off-gases. The first important commercial applications of monolithic catalysts were for decolorization of nitric acid tail gas and for car exhaust emission control. The main reasons for focusing research on monoliths was their low-pressure drop, low sensitivity to plugging and high mechanical strength.[13] By 1975, the first cars equipped with catalytic converters became available. Monoliths are available made from different materials, and an interesting application of metal monoliths is for controlling heat removal in packed beds due to their superior heat transfer characteristics compared to those of ceramic monoliths.[14] Thus, metal monoliths can be applied when a thorough control of the temperature in tubular reactors is needed.

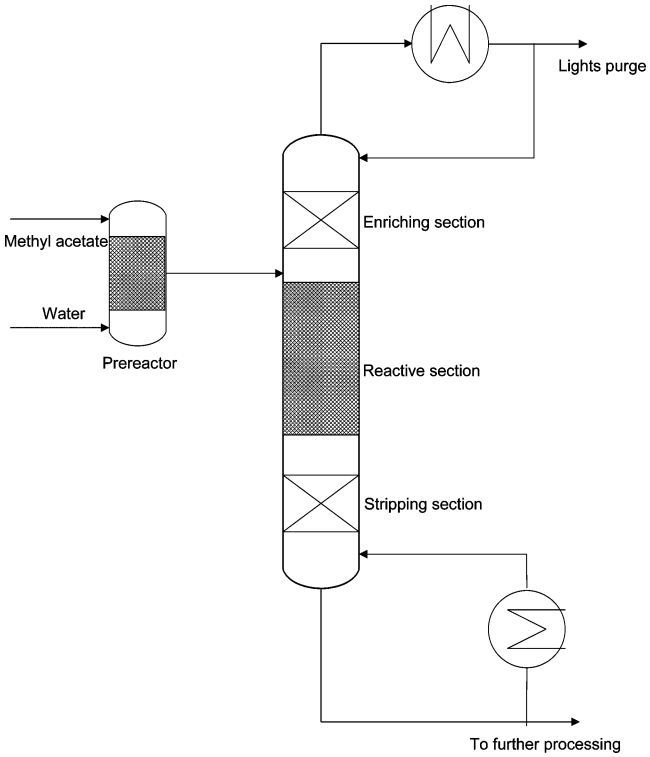

Figure 2. Flow sheet of the reactive distillation process for methyl acetate hydrolysis.[13]

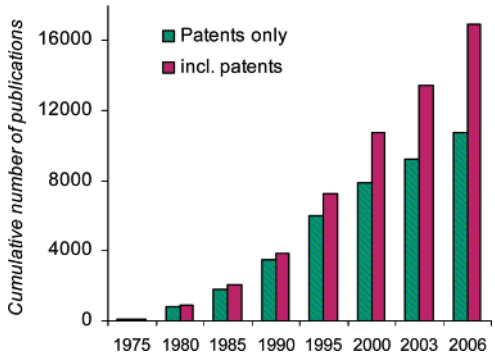

Figure 3. Number of publications with the word "monolith" or "honeycomb" in the title. The patent category includes patent applications (data obtained from www.ISIKnowledge.com).

Comprehensive reviews on catalytic combustion, including the use of monoliths for automotive converters, have been published in the past few decades.[15−17] Reviews on monoliths including nonenvironmental and noncombustion applications of monoliths

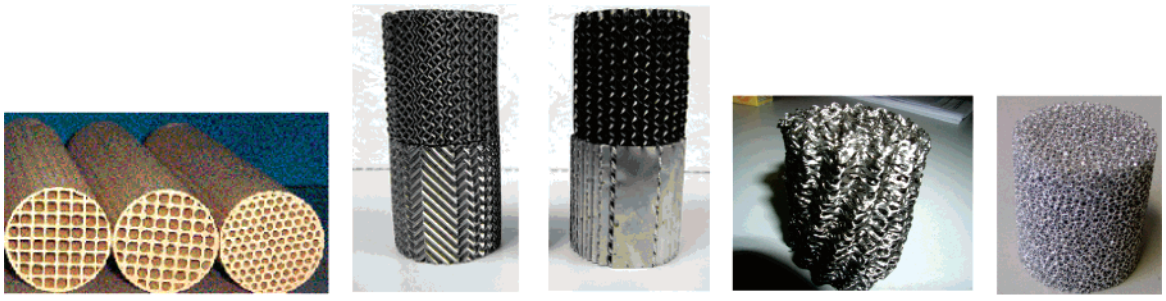

Figure 4. Cordierite monoliths: (a) square, rounded corners, hexagonal channels; (b) open crossflow structure; (c) closed crossflow structure; (d) knitted wire packing; (e) aluminum foam.

have also been published.[6,18] The increasing interest in monolithic catalysts is reflected in the literature. The number of publications on monoliths and/or honeycomb structures (see Figure 3) is rising almost exponentially. It is striking that the fraction of patents is over two thirds. Lately, cellular metallic foams have seen increased application as an excellent thermal management material. An example of such applications is the use of metal foams as compact heat sinks for cooling of microelectronic devices such as computer chips or power electronics.[19] A unique graphitized foam developed at the Oak Ridge National Laboratory (ORNL) promises more efficient and compact heat exchangers.[20] The foam combines a high heat conductivity, porosity and geometric surface area due to which the overall heat transfer coefficients of foam-based heat exchangers can be up to 2 orders of magnitude greater than conventional heat exchangers.[20]

Apart from these there are number of structured packings that have proven to be successful at laboratory scale from either mass transfer or heat transfer point of view but yet have to be commercialized. Details of these packings can be found in Wen et al.[21] and Kolodziej et al.[22]

In this review, we will discuss a number of commercially available structured packings as potential structures that can be applied for multiphase catalytic reactions. They can be classified in the following categories.

(1) Monoliths are the first category, which are structures of parallel straight channels, with typical characteristics of low-pressure drop, high porosity, high geometric surface areas.[6] Monoliths can be ceramic (cordierite) or metal based (copper, aluminum, etc.). The heat transfer characteristics of ceramic based monoliths are poor compared to metal based monoliths, due to their low heat conductivity.

(2) Corrugated sheet/gauze packings are the second category, which can be subdivided into the following two categories:

(2a) The open cross flow structure (OCFS), which consists of corrugated sheets stacked parallel to each other, and whose corrugation orientation is alternately inclined to the axis. Typical characteristics are low pressure drop, high porosity, high geometric surface areas, and efficient radial mixing.[23] These packings are manufactured as metal sheet or metal wire gauze packings both available commercially. Examples of metal sheet packings are Katapak-MK or Mellapak and that of wire gauze packings is Sulzer BX, all manufactured by Sulzer.[24]

(2b) The closed cross flow structure (CCFS) contains an additional flat plate between the corrugated sheets, forming closed channels inclined to the axis. Typical characteristics are low-pressure drop, high porosity, high geometric surface areas and mixing at the wall, thus allowing efficient heat transfer from the packing to the outside of the reactor.[25] They are not (yet) commercially manufactured.

(3) Knitted wire packing is the next category, which consists of knitted multiple fine metallic filaments that are then crimped and spirally wound. Typical characteristics are low-pressure drop, high porosity, and high geometric surface areas. Radial mixing properties and heat transfer performance of these packings are unexplored as yet.[26]

(4) Open-celled foams yield the final category, which are 3D cellular materials made of interconnected solid struts (pores), forming a sponge type tortuous path network. Typical characteristics are low- and high-pressure drop, high porosity, high geometric surface areas, and good heat transfer characteristics.[27,28]

Figure 4 gives typical examples.

As a whole, these packings provide additional degrees of freedom with respect to pressure drop, porosity, catalyst hold-up etc. An appropriate example is the variation of catalyst hold-up without having an equivalent effect on the pressure drop. Depending on the application, the catalyst hold-up in a structured packing can be simply varied over a broad range by manipulating the coating thickness. Filling the channels of the packing with catalyst particles is an alternative solution for increasing the catalyst hold-up.[4,29] Thus, structured catalysts offer greater flexibility with respect to catalyst hold-up compared to a packed bed.

5. Transport Phenomena in Random and Structured Fixed Bed Reactors: Hydrodynamics, Mass Transfer and Heat Transport.

Extensive reviews of hydrodynamics and transport parameters in trickle bed reactors have been published.[1−3,30−32] The most important parameters such as flow regime, pressure drop, liquid hold-up, gas to liquid mass transfer coefficient and gas−liquid interfacial area and heat transport from the packed bed to the heat transfer fluid are outlined in this section. It will be clear that not only catalyst development but also hydrodynamics and mass and heat transfer studies are of prime importance for a proper evaluation of the various reactor types and for creation of an optimal reactor performance.[4]

5.1. Flow Regimes. Under the conditions employed in industrial co-current trickle-bed reactors, two types of flow regimes can be encountered: the low interaction and the high interaction regime.[33] The low interaction regime consists of trickle or film flow and the high interaction regime consists of spray, pulse and bubble flow.[34] The majority of the co-current fixed bed operations are carried out in the trickle flow regime.

In analogy to randomly packed bed reactors, two distinct flow regimes can be observed in structures with closed channels (e.g.,

monoliths and closed crossflow packings): film flow and slug or Taylor flow. Film flow is characterized by films covering the channel walls with only low interaction between gas and liquid.[35] Taylor flow consists of gas bubbles and liquid slugs flowing consecutively through the small monolith channels. The gas bubbles occupy the whole cross section of the channel and are elongated. Only a thin liquid film separates the gas bubble from the catalyst.[36] Such a flow pattern is associated with high gas to liquid mass transfer rates as will be evident in the subsequent sections. A gas to liquid ratio between one and three typically leads to stable Taylor flow with liquid superficial velocities ranging from 0.05 to 0.15 m/s and channel diameters of less than 2 mm.[37]

Since a coated structure will have a much lower catalyst loading (~20%) compared to a randomly packed bed (~60%), it is extremely important to aim for high geometric surface areas for the coated structures. For this, the channel dimensions of the structure should be in the order of mm. This is sufficient to facilitate the Taylor flow pattern provided the gas and liquid velocities are in the right ranges. Because of the high mass transfer rates associated with Taylor flow, it is the most preferred regime of operation for fast reactions that are mass transfer limited. Since Taylor flow requires high liquid velocities, structured packings having low-pressure drop can be easily operated in this flow regime.

Thus, the flow regimes most likely to occur in monolith and closed channel packings are film flow (at low liquid velocities and intermediate gas velocities) and Taylor flow (at high liquid velocities and intermediate gas velocities). For corrugated packings, foams and multifilament wire mesh packing, trickle flow (at low liquid velocities and intermediate gas velocities) and pulse flow regimes (at high liquid velocities and high gas velocities) can be found.

5.2. Pressure Drop and Liquid Holdup. The estimation of liquid hold-up is of great interest as it has a strong influence on pressure drop, catalyst wetting, and heat transfer. Pressure drop is important in determining the energy losses, sizing of the compression equipment etc. At a given gas density, the two-phase pressure drop increases with gas and liquid mass fluxes, liquid hold-up and liquid viscosity. Liquid hold-up increases with liquid superficial velocity and liquid viscosity and decreases with increasing gas density and gas superficial velocity.

Two basic approaches to describe the hydrodynamics of a packed bed reactor are the channel model and the particle model.[38] In the channel model, the gas is assumed to flow inside numerous small channels having a characteristic dimension; as liquid flows down the "walls" of the same channels it reduces the available cross-sectional area for gas flow, thus causing increased pressure drop. In the particle model the gas is assumed to flow around a packing particle having a characteristic dimension and the liquid acts to increase this dimension by its adherence to the particle surface. The presence of the liquid also reduces the void fraction of the bed.

5.3. Gas—Liquid Mass Transfer and Interfacial Area. Gas−liquid mass transfer resistance can have a detrimental effect on the reactor performance. Therefore, accurate estimation of the mass transfer parameters is important for achieving successful reactor design and scale-up. In principle, for a given pressure, temperature and gas−liquid system, the mass transfer coefficient k_L is generally a function of the diffusivity of the gas in the liquid and renewal rates of the liquid phase. As a consequence, it is largely dependent on the level of turbulence occurring in the reactor and hence the type of reactor. For a given gas density, the gas−liquid interfacial area increases with liquid mass flux and velocity. In film flow, improved spreading of the liquid film over the whole geometric area of the packing is a key factor in improving the gas−liquid interfacial area for mass transfer. Although turbulence is not relevant in Taylor flow operated monoliths, at increasing flow rates the gas to liquid mass transfer rate increases. This is because, though Taylor flow occurs under laminar flow conditions, the recirculation patterns in the liquid slugs enhances transfer of gas from the caps of the bubbles to the liquid slug.

Very high values of gas−liquid mass transfer rates are achieved in Taylor flow operated monoliths.

5.4. Liquid—Solid Mass Transfer. The rate of mass transfer of the reactants and products from liquid to catalyst particle surface is very important and needs to be accounted for in evaluating trickle bed reactor performance.[39] Liquid hold-up and pressure drop affect the interstitial gas and liquid velocities which have a direct influence on the mass transfer coefficients and catalyst wetting efficiency.[39] External catalyst wetting efficiency is an important design and scale-up parameter in determining the degree of catalyst utilization in trickle bed reactors.[3] Generally speaking, pressure and gas velocity have a positive effect on the catalyst wetting efficiency. This is because the liquid film thickness at a fixed liquid mass velocity decreases with pressure and gas velocity. This results in an improved spreading of the liquid film over the external packing area.[3] The same cannot be said for monoliths operated in the Taylor flow regime. In Taylor flow, which is a surface tension dominated flow regime, high gas velocity leads to increased film thickness and as a consequence decreases the liquid−solid mass transfer.

5.5. Residence Time Distribution (RTD). In real flow systems the flow pattern is intermediate to the two extremes of plug flow and back mixed (CSTR) behavior.[40] This deviation from ideal flow conditions can be attributed to channelling and dead zones. Therefore, the usual assumption of plug flow in packed columns may not be correct in all instances.[41] In Taylor flow, the dispersion is low because the gas bubbles seal the liquid slugs. The only dispersion mechanism is the exchange with the stationary film. However, on the scale of the reactor the differences in residence time distributions between the channels have to be taken into account. Very important is the inlet design.

Back mixing commonly termed as "axial mixing" is detrimental to the performance of multiphase reactors in the case of positive order reactions, especially at high conversions, or for consecutive reaction schemes where selectivity is the main issue.[42] This is because axial mixing reduces the driving force for mass transfer, heat transfer and reaction and usually additional height needs to be allowed for to achieve a given transfer rate in physical processes, e.g., distillation or conversion in chemical processes.[41] It is well-known that the liquid-phase flow pattern in a packed column does not deviate significantly from plug flow, and therefore the dispersed plug flow model has been widely used to describe it.[40]

RTD is a powerful tool to analyze the axial mixing and hydrodynamic behavior of the fluids in the reactor.[43,44] The variance of RTD of the reactor indicates the deviation from ideal plug flow.[43] It is a strong function of the flow patterns prevalent in a certain reactor type.

Generally a narrow residence time distribution is desired.

5.6. Heat Transport. Reactions, which are characterized by a large heat evolution and selectivity problems, are often carried out in wall-cooled packed bed reactors. The heat of reaction is removed from the reactor by a cooling agent, e.g., evaporating steam. The complex heat transfer phenomena in packed beds with co-current gas−liquid flow have been extensively analyzed

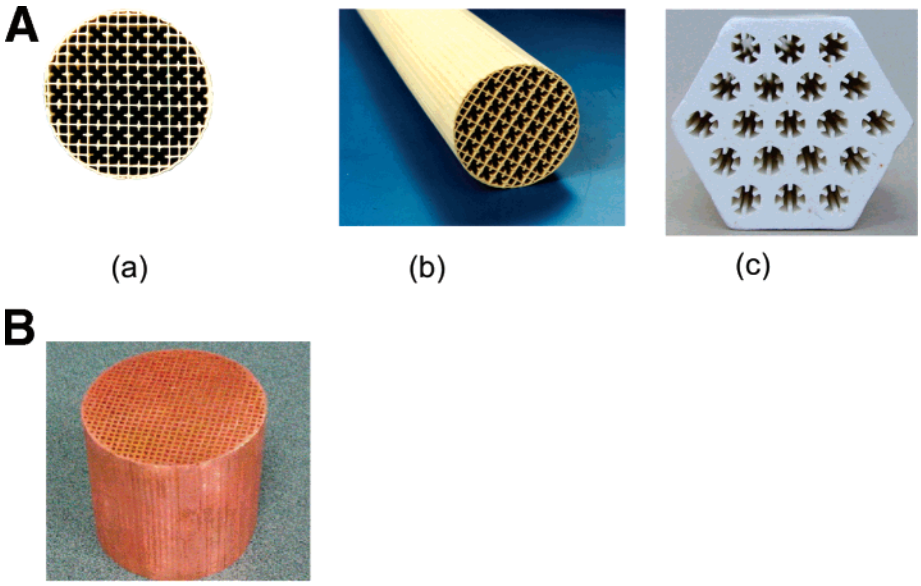

Figure 5. (A) Internally finned monoliths (a and b, Corning, Inc., New York; c, ECN, Petten). (B) Copper-based monolith with square channels.[14]

Table 2. Typical Geometric Properties and Hydrodynamic Regime of Monoliths

cell density (cpsi)	25	50	100	25	200	400	600
GL flow type	film	film	film	film	Taylor	Taylor	Taylor
channel shape	square	square	square	square finned	square	square	square
void fraction (%)	67	68	69	73	74	75	79
surface-to-volume ratio (m^2/m^3)	654	939	1312	1040	1900	2800	3500
hydraulic diameter (mm)	4.12	2.91	2.1	2.8	1.56	1.08	0.9

in the literature and several models have been developed in order to describe heat transfer in the bed.

The most widely used model is the 2-D pseudo homogeneous plug flow model in which two main assumptions are made:

(1) At any location of the reactor, all three phases (gas, liquid, solid) are at the same temperature.

(2) Plug flow conditions exist for the gas and liquid phases.

The model contains two parameters: the effective bed radial conductivity, $\lambda_{e,r}$ which determines the amount of heat that can be transferred from the bed to the vicinity of the tube wall and the wall heat transfer coefficient, α_w, which allows taking into account a poorer heat transfer close to the wall. On the one hand $\lambda_{e,r}$ for structured packings is typically larger than that for randomly packed beds. This is due to the significant contribution of the radial convection component in addition to the improved static conductivity which depends mainly on the geometry of the matrix and the conductive properties of the material, e.g., copper monolith, aluminum foam, etc. On the other hand, α_w is expected to be smaller in the case of structured packings, due to a defined gap present between the skin of the packing and the tube wall. The gap constitutes the main thermal contact resistance for the heat transfer from the packing to the coolant.

Various approaches used in literature to describe the flow patterns, pressure drop, liquid hold-up and transport rates in the structures mentioned above are critically discussed in the subsequent sections.

Though multiphase reactors are usually operated in the gas−liquid down-flow mode, data obtained for the structured packings in counter-current mode is included in this review. Counter-current operation is relevant in order to bring out similarities between co-current and counter-current flow modes in the low-interaction regime. A good example to demonstrate this are the phenomenological correlations developed for structured packings tested in a counter-current flow mode which can be applied to co-current flow mode provided the flow patterns in both cases are similar for, e.g., liquid flowing down the wall as a film and gas flowing through the central core of the channel. Moreover, a major application of structured catalysts is in catalytic distillation, where counter-current flow is dominant.

Furthermore, heat transfer and pressure drop correlations for gas phase only are also included for foams, static mixers and metal monoliths where two-phase data are not available. The single-phase models can be used as starting point for modeling pressure drop and heat transfer rates for multiphase applications.

6. Structured Internals

6.1. Monoliths: Ceramic and Metal. Monoliths are ceramic or metallic blocks containing parallel, straight channels. The open structure without bends hardly obstructs flow, yielding a low-pressure drop. The size of the channels is usually small, and is characterized by the cell density in cells per square inch (cpsi).[6] On the walls of the channel a thin layer of catalytically active material can be deposited. In this way, a high external surface area and a short diffusional distance are obtained.[4] The material of construction includes various ceramics as well as metals. Ceramic monoliths have been used extensively in gas−solid applications such as the automotive exhaust converter and deNOx reactors.[6] Monoliths are being increasingly considered as an interesting alternative for gas−liquid−solid applications.[4] The only current large scale gas−liquid−solid commercial application of monoliths is the hydrogenation of anthraquinone in hydrogen peroxide production.[45] Reviews on hydrodynamics and transport phenomena in multiphase monolith reactors have been published.[46,47]

Ceramic monoliths are commercially available in different channel shapes and sizes, the most common being square, hexagonal, and triangular (see Figure 5A). Extruded metal monoliths made out of copper are developed by Corning

Incorporated to promote radial heat transfer mainly by conduction (see Figure 5B). Internally finned monoliths, invented at TUDelft, with larger channel diameters have been designed mainly for countercurrent operations.[48] The internal fins create separate paths for the gas and the liquid and also contribute to the catalyst hold-up. Typical geometric properties of the various monoliths are given in Table 2.

Different techniques of applying catalyst support material and active catalyst on a monolith body are discussed in literature.[49−51]

Table 3 lists the experimental details of the studies on hydrodynamics; mass transfer and heat transfer in monoliths along with the respective correlations reported.

For the monolith reactor a good liquid distribution at the entrance is crucial because in the reactor radial transport is not possible due to the absence of flow exchange between the channels. Once a good distribution is ensured all the monolith channels can be utilized for mass transfer and reaction. Therefore, the selection and design of the appropriate distributor and its positioning is a major challenge. Correctly positioned spray nozzles have been proven to provide distributions far better than the conventional distributors used for trickle beds.[35] Stacking of monoliths can improve mass transfer performance in processes which are limited by intraparticle diffusion or when viscous or foaming liquids are present due to the radial remixing of the laminar layers.[52]

Flow regime transition measurements were done in a monolith with 1.5 mm square channels using a conductivity probe measurement method.[53] Figure 6 shows a flow map, which represents the flow transition from film flow to slug flow. The correlation developed from these flow transitions is given in Table 3. Since the flow transitions have been determined for a specific system, i.e., a monolith with 1.5 mm square channels, aqueous liquid, it is uncertain whether this correlation can be extended to other systems For example, a monolith with circular channels will show flow transition at other gas and liquid velocities than square channels due to lower cross-sectional area and due to the fact that in square channels the gas−liquid interaction is lower as liquid retracts in the corners of the channel. Similarly, the flow transition will take place at lower gas and liquid velocities when fluids of higher viscosity are used.

Liquid hold-up measurements are reported for monoliths operating in the film flow regime. An empirical correlation derived from the classical Nusselt theory for smooth laminar falling films along a vertical surface was proposed by Heibel et al.[35] for the dynamic liquid hold-up in film flow monolith (see Table 3). This correlation is in good agreement with the previously reported correlation of Lebens et al.[48] (see Table 3) for internally finned film flow monoliths. The correlation predicts a strong dependence of β_L on the hydraulic diameter of the monolith channels. Thus, the higher the geometric surface area, the higher would be the liquid hold-up. This is logical, as higher surface areas would lead to higher coverage of the channel wall, and eventually lead to higher hold-up. It is worthwhile to note the applicability of this correlation to low surface tension liquids and liquids with higher viscosities.[35] Figure 7 shows a plot of the liquid hold-up as a function of Reynolds and Froude number for two different channel diameters and two different systems. The effect of gas flow rate on the liquid hold-up is limited. Therefore, the correlation takes into account the effects of the liquid phase and gas-phase effects can be neglected. In general, the correlation can be applied to predict liquid hold-up in any monolith geometry for any kind of liquid.

The pressure drop model for film flow monoliths proposed by Lebens et al.[54] is based on a phenomenological approach, originally used for randomly packed beds (see Table 3). The approach is based on the pressure loss in a dry bed of particles and how it is affected by the presence of the liquid. An important feature of this work is that it takes into account the effect of liquid hold-up on pressure drop and vice versa. The model predicted the data within ±20%, thus proving that such models based on physical phenomena can describe the irrigated pressure drop in monoliths rather well. Figure 8 is a plot for the irrigated pressure drop in which the experimentally obtained wet pressure drop is compared with the phenomenological model for a square finned channel. The constants in the correlation depend on the channel geometries.

Kreutzer et al.[55] developed a semiempirical model for pressure drop of Taylor flow in monoliths based on quantifiable features of the flow pattern, so that experimental pressure drop data can be used to characterize the flow pattern (see Table 3). The model was verified by determining the slug length experimentally and comparing it with the value obtained from the pressure drop model at a given liquid hold-up (see Figure 9). The agreement of the slug length obtained from pressure drop and the slug length obtained from conductivity measurements is very good. As seen in Figure 10, for long slugs ($\epsilon_L \rightarrow 1$) the value of fRe approaches the limit value for infinitely long slugs (16 for square geometry and 14.2 for circular geometry) and the method loses its sensitivity.[56]

k_La_e values measured by various authors in monoliths are given in Table 4.

Lebens et al.[57] and Heibel et al.[58] carried out measurements in the film flow regime to determine the effect of monolith length on k_La_e. The results of Lebens et al.[57] show that the mass transfer is significantly higher in the first part (0−0.25 m) of the monolith than in the other two sections. The development of both velocity and concentration profile leads to a strong enhancement of the mass transfer at the inlet. The end effects need to be deduced for the determination of k_La_e of the considered monolith section as they are not measured in the developed flow regime. Thus, the k_La_e values of the section 0.25−0.5 m should be considered for further analysis and comparison. Heibel et al.[58] performed measurements in the film flow regime in both co-current and countercurrent mode and showed that the mode of operation, i.e., co- or countercurrent film flow, has no influence on the mass transfer rates. This corroborates the conclusion that the film reactor operates in a low-interaction regime.

Heiszwolf et al.[36] measured k_La_e in slug flow regime and compared the data with the k_La_e values obtained from the correlation of Bercic and Pintar[59] using different values of the slug length. The data were well correlated at high liquid velocities ($u_L > 0.1$ m/s, see Figure 11). The observation that the correlation was not satisfactory at low flow rates can be due to the fact that at a too low liquid velocity no slug flow can be established in the channels because of hydrodynamic instabilities.[60] So, it is understandable that the model, derived for the slug flow regime, fails to describe the mass transfer process at low liquid velocities. The model of Bercic and Pintar[59] may be applied to obtain k_La_e in the slug flow regime provided that the liquid slug length is known. It is striking that k_La_e values obtained are in the range 0.4−1 s^{-1}, remarkably high if compared to the values obtained in trickle bed reactors (∼0.1 s^{-1}).

Table 3. Correlations for Hydrodynamic and Transport Parameters for Monoliths

reference	correlations	method	geometric properties	operating conditions	comments
Heibel and Lebens[53]	flow transition: slug flow to film flow $u_{G,trans} = -3.5 + 5.0(u_{L,trans} \times 100)^{0.3}$	measuring the conductivity using platinum microprobes, aqueous NaCl, and air	150 mm long 1.5-mm square channels 42-mm-diameter cordierite	co-current down flow $\mu_L = 0.5-6$ m/s $\mu_G = 0.5-6$ m/s	validated using aqueous systems, can be extended to other systems
Lebens et al.[57]	gas−liquid interfacial area in film flow $a_e = 2673\sqrt{\beta_L} \vee \beta_L < 0.147$ $a_e = 1112 - 704\,\beta_L \vee 0.147 < \beta_L < 0.25$ a_e is based on the volume of the void space	modeling	1 m long 4.62-mm square channels with fins 43-mm-diameter cordierite	valid for μ_L up to 0.055 m/s for water	2-D Poisson-type PDEs which define the velocity profile
Heibel et al.[35]	liquid holdup in film flow $\beta_L = 6.6\left(\frac{Fr_L^2}{Re_L}\right)^{0.46}$	magnetic resonance imaging, water, 10% and 25% aqueous sucrose solution	0.5 m long 2.91- and 4.11-mm square channels 42-mm-diameter cordierite	co-current down flow $\mu_L = 0.01-0.04$ m/s $\mu_G = 2.7$ m/s	effect of surface tension and viscosity studied $\beta_L \propto 1/d_h^2$
Lebens et al.[48]	liquid holdup in film flow $\beta_L = 6.95\left(\frac{Re_L}{Ga_L}\right)^{0.46} \vee \beta_L < 0.25$	weighing technique: static and dynamic hold-up, water, *n*-decane, and 20% aqueous sucrose solution	1 m long 4.62-mm square channels with fins 43-mm-diameter cordierite	$\mu_L = 0.005-0.06$ m/s, no gas flow	
Lebens[54]	pressure drop in film flow $\phi^2(1-\beta_L)^n = 1 - \frac{B_2\sqrt{Re_L}}{Fr_G}\,\phi^2 = \frac{\left(-\frac{dp}{dz}\right)_{irrigated}}{\left(-\frac{dp}{dz}\right)_{dry}}$ $B_2 = 0.081$, $n = 2$ for circular tube $B_2 = 0.045$, $n = 0.87$ for circular finned tube $B_2 = 0.049$, $n = 1.5$ for square finned tube	differential pressure transmitter, water and air	1 m long 4.62 mm square channels with fins 43-mm-diameter cordierite	countercurrent $\mu_L = 0.005-0.06$ m/s $\mu_G = 0.2-2$ m/s	
Kreutzer et al.[55]	pressure drop in Taylor flow $fRe = \frac{(\Delta p/L - \rho_L g\epsilon_L)d^2}{2\mu_L(u_L+u_G)\epsilon_L} = 16\left[1 + \frac{0.17d}{L_{slug}}\left(\frac{Re}{Ca}\right)^{1/3}\right]$ (for circular channels) $= 14.2\left[1 + \frac{0.17d}{L_{slug}}\left(\frac{Re}{Ca}\right)^{1/3}\right]$ (for square channels)	measuring the conductivity using platinum microprobes, aqueous NaCl, and air	300 mm long 1.5-mm square channels 100-mm-diameter cordierite	co-current down flow $\mu_L = 0.02-0.2$ m/s $\mu_G = 0.02-0.3$ m/s	
Lebens et al.[57]	gas−liquid mass transfer in film flow $Sh_{ave} = 1.04 + 0.35(1/Gz)^{-0.63}Gz = \frac{\delta^2 u_L}{ZD_L}$	desorption of oxygen from saturated water into nitrogen	1 m long 4.62-mm square channels with fins 43-mm-diameter cordierite monolith	countercurrent $\mu_L = 0.005-0.03$ m/s $\mu_G = 0.2-1$ m/s	semitheoretical correlation
Bercic and Pintar[59]	gas−liquid mass transfer in Taylor flow $k_L a_e = \frac{0.133\mu_{TP}^{1.2}}{L_{slug}^{0.57}}$	physical absorption of methane in water	1.12 m long glass capillary with 1.5, 2.5, and 3.1 mm i.d. 0.6 m long glass capillary	co-current down flow $\mu_L = 0.01-0.4$ m/s $\mu_G = 0.01-0.4$ m/s	empirical correlation, no dependence found on channel dimensions
Irandoust et al.[61]	gas−liquid mass transfer in Taylor flow $k_L a_e = 4[\delta(d_c - \delta)u_{ave,film}y_m + D_L Sh_L d_b]/[d_c^2(L_{slug} + L_{bubble})]$ $Sh_L = \frac{k_L d_b}{D_L}$	absorption of oxygen from air into water, ethanol, and ethylene glycol	with 1.5 and 2.2 mm i.d.	co-current up flow $\mu_L = 0.092-0.56$ m/s $\mu_G = 0.01-0.4$ m/s	theoretical correlation, validated with experimental results

Table 3. (Continued)

reference	correlations	method	geometric properties	operating conditions	comments
Bercic and Pintar[59]	liquid−solid mass transfer in Taylor flow $Sh_{LS} = 3.51\left(\frac{ReSc}{l/d_{cap}}\right)^{0.44}\left(\frac{L_{slug}}{d_{cap}}\right)^{-0.09}$	dissolution of benzoic acid into water, measuring dissolved benzoic acid using refractory index detector	25−35 cm long coated tubes with 2.5 mm i.d.	$\mu_L = 0.01-0.4$ m/s	L−S mass transfer increases with liquid velocity, L_{slug} important parameter for determining L−S mass transfer
Kreutzer et al.[62]	liquid−solid mass transfer in Taylor flow $k_{LS} = \frac{1}{\frac{1}{D_L/d_h 20(1+0.003)\left(\frac{\psi_L}{Re_L Sc}\right)^{-0.7}} + \frac{1}{D_i/\delta}}$ $\delta = d_h 0.18(1 - e^{-3.08Ca0.54})$, $Ca = \frac{u_{TP}\mu_L}{\sigma_L}$, $a_{LS} = 4/d_c$	liquid to solid heat transfer modeled with CFD simulations performed for a 1-mm-diameter cylinder with a moving wall, for mass transfer with *Sh*	−		model validated with data from Bercic and Pintar[59]
Heibel et al.[63]	residence time distribution of the liquid in film flow no correlation developed	dynamic response absorbance measuring technique, air/water system, Ecoline blue ink as tracer	0.5 m long 25 cpsi square channels 43 mm diam cordierite monolith	co-current down flow $\mu_L = 0.023$ m/s	effect of maldistribution studied
Yawalkar et al.[42]	residence time distribution of the liquid in Taylor flow $Pe_f = 3.268 \times 10^{-3} Re^{0.31} \beta_{G,Taylor}{}^{-0.95} \psi_L{}^{-0.23}$	same as above	0.5 m long, 200-, 400-, and 600-cpsi square channels 43-mm-diameter cordierite monolith	co-current down flow $\mu_L = 0.05-0.1$ m/s $\mu_G = 0.07-0.13$ m/s	effect of channel and inter-monolith redistribution studied, axial mixing lower in down flow than in up flow mode
Groppi and Tronconi[64]	effective radial thermal conductivity in gas−solid systems $\lambda_{e,r} = \lambda_s \left(\frac{(1-\sqrt{\epsilon+\xi}) + \frac{\sqrt{\epsilon+\xi}-\sqrt{\epsilon}}{1-\sqrt{\epsilon+\xi}+\frac{\lambda_w}{\lambda_s}\sqrt{\epsilon+\xi}}}{} + \frac{\sqrt{\epsilon}}{(1-\sqrt{\epsilon+\xi}) + \frac{\lambda_w}{\lambda_s}(\sqrt{\epsilon+\xi}-\sqrt{\epsilon}) + \frac{\lambda_w}{\lambda_s}\sqrt{\epsilon}} \right)$	based on theoretical analysis	−	−	theoretical correlation

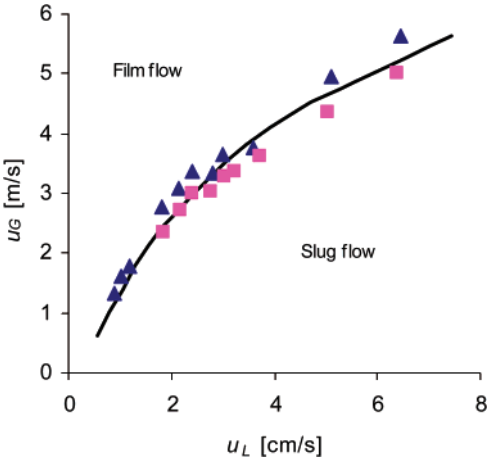

Figure 6. Flow map of film flow to slug flow (water/air) for a monolith (1.5 mm square channels, length of 150 mm), based on the conductivity test method.[53] The line represents the equation in Table 3.

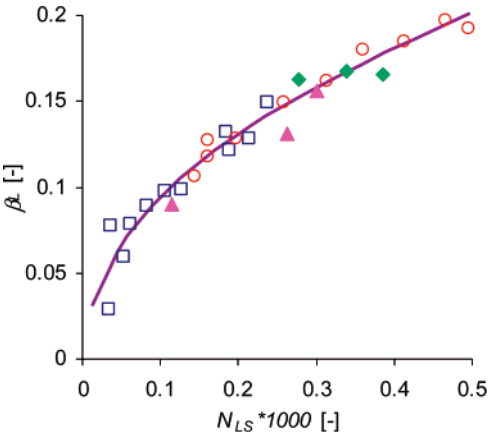

Figure 7. Liquid holdup for a 25-cpsi monolith under film flow conditions, as a function of the dimensionless number for the liquid, $N_{LS} = Fr_L^2/Re_L$: (□) water; (▲) 10% sucrose in water; (◆) 25% sucrose in water; (○) 50 cpsi monolith for water; (line) correlation described in Table 3.[35]

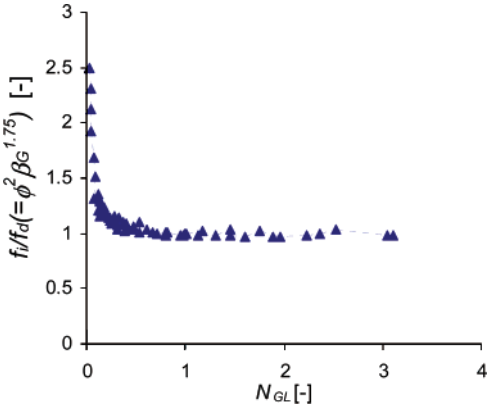

Figure 8. Irrigated pressure drop (i.e., pressure drop in the presence of liquid) under film flow conditions for a square finned channel compared to the phenomenological model.[54] The line represents the phenomenological correlation derived based on the "channel model". f_i and f_d represent the friction factors for the irrigated and dry system respectively, ϕ^2 = dimensionless pressure gradient ratio and β_G = the fraction of the void space filled with gas. $N_{GL} = Fr_G/Re_L^{0.5}$.

Heibel et al.[63] reported RTD curves for monolith operated in co-current down flow with film flow for conditions with and without maldistribution inside the channels. A $D_{ax,L}$ value of around 0.01 m^2/s was obtained from the curves. They found that due to the channel scale maldistribution effects a slight shift

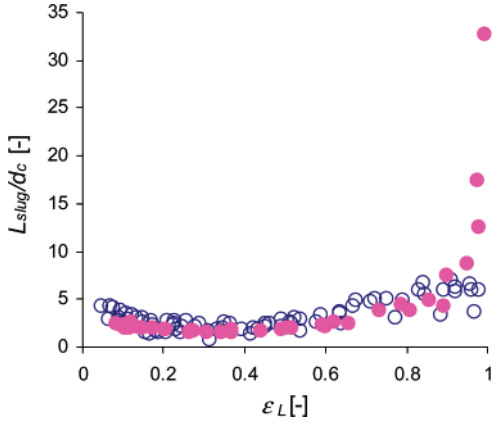

Figure 9. Slug length versus liquid holdup for the coarse shower-head distributors used on a 200-cpsi square-channel monolith (0.1 m diameter) determined (●) directly by conductivity and (○) indirectly from the pressure drop.[55]

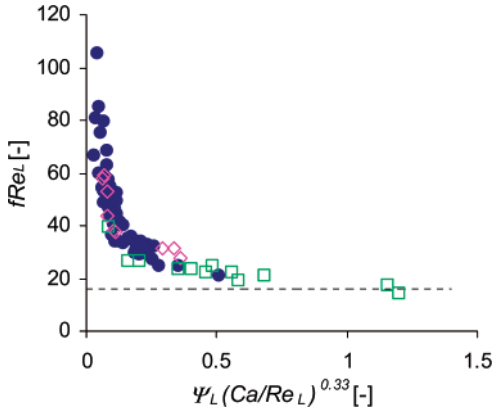

Figure 10. Pressure drop correlation (fRe_L as a function of the dimensionless group, $\Psi_L(Ca/Re_L)$ for Taylor flow, Ψ_L = dimensionless slug length (for gas liquid flow in a round capillary with channel diameter d_c = 2.3 mm): (●) air/water; (○) air/decane; (□) air/tetradecane; and (- - -) the single-phase limit.[56]

of the mean residence time occurred to lower values (see Figure 12). Not only this but broadening of the residence time distribution was also observed, which is of course not desirable from reactor performance standpoint. Therefore, as stressed earlier, a well-designed liquid distributor is important not only to distribute the liquid evenly over the channels but also to reduce axial dispersion.

Similarly Kreutzer et al.[65] have remarked that although the extent of back-mixing under Taylor flow conditions in a single channel is in general minimal, the same does not necessarily hold for a monolith column. If the distribution of gas and liquid inside the monolith channels is not perfect, the velocity of the slugs and bubbles can vary from channel to channel. Monoliths are a special case because there is no flow from channel to channel so unlike randomly packed bed reactors or other structured packings, redistribution inside the packing is impossible. As redistribution inside the packing cannot flatten out a feed maldistribution, it is no surprise that previous studies,[59,66] have shown more severe backmixing in monolith reactors in comparison to trickle-bed reactors. Yawalkar et al.[42] found $D_{ax,L}$ values between 0.004 and 0.014 m^2/s for the 200, 400, and 600 cpsi monoliths operated in co-current down flow with Taylor flow conditions. They concluded that degree of axial mixing decreased with decrease in channel size. Inter-monolith redistribution, i.e., stacking of monolith elements, was found to decrease not only the maldistribution effects but also axial

Table 4. $k_L a_e$ Values Obtained in Film Flow and Slug Flow Regime in Monoliths

	flow regime	monolith geometry	$k_L a_e$ (s^{-1}) (for different monolith lengths, based on the reactor volume (in m^3))
Lebens et al.[57]	film	4.6 mm, square channels with fins	0.02−0.08 (0.25 m) 0.01−0.03 (0.25−0.5 m) 0.005−0.01 (0.5−1 m)
Heibel et al.[58]	film	4.1 mm square channels	0.005−0.015 (0.08−0.5 m)
Heiszwolf et al.[36]	slug	1.5 mm, square channels	0.4−1 (1 m)

mixing. The corner flow of the liquid in the square channels leads to tailing of the RTD curves (see Figure 13) thereby leading to significant axial dispersion. This effect can be reduced by using rounded or circular channel monoliths where the amount of corner flow is significantly low.

A comparison between the $D_{ax,L}$ values in the two flow modes tells us that axial dispersion in film flow is higher than in Taylor flow, the reason being the larger channel sizes giving rise to a different flow pattern and the much lower liquid flow rates employed to achieve film flow.

The issue with monoliths is that by maldistribution and laminar flow profiles the RTD gradually shifts from a stochastic to a deterministic determined phenomenon, meaning that the dimensionless RTD does not sharpen up with reactor length as is the case with a stochastic process. Therefore, special care must be taken to avoid maldistribution in structured systems that are sensitive to this aspect.[65]

Determination of heat transport from the packing to the heat transfer fluid is extremely relevant for exothermal multiphase reactions. Work has been done comparing ceramic monoliths and highly conducting monoliths, e.g., copper monoliths. Unfortunately, until now only gas-phase studies have been employed for studying heat transfer rates in monoliths. For ceramic (cordierite) monoliths severe radial temperature gradients were observed, obviously due to the strong resistance to heat transport of the ceramic material to the heat transfer fluid.[14] Typically, radial convection is absent in monoliths and conduction of ceramic monoliths is not sufficiently high to facilitate considerable radial heat transport. In contrast, metal monoliths due to their good heat conduction properties can provide considerable radial and axial heat transport.[67] If suitable materials and geometries are adopted, then the heat conduction through the monolith matrix can become quite significant.[67]

Groppi and Tronconi[64] have derived a predictive equation for the effective radial thermal conductivity (see Table 3) based on a theoretical analysis of heat conduction in the unit cell of the monolith catalyst. Figure 14 shows the effect of material properties and monolith void fraction on the estimated effective radial thermal conductivity. Thus, values of $\lambda_{e,r}$ greater by 1 order of magnitude than those for packed beds (2−5 W/(m K)) can be obtained. Metal monoliths have excellent radial heat transfer properties, and as a consequence, they have a high potential as reactor base for strongly exothermic reactions. Tronconi et al.[14] performed experiments with different monolith materials to explore the differences in radial thermal conductivity. The influence of the material properties is evident in parts a and b of Figure 15, representing the axial temperature profile at different radial positions inside a cordierite and copper monolith respectively. Clearly, the much higher thermal conductivity of the copper monolith compared to the cordierite has a large impact on the radial transport of heat. It is not surprising that a large resistance to heat transfer lies between the skin of the packing and the inner reactor wall. Therefore, the difference between the copper and cordierite monolith in terms of the overall heat transfer coefficient is reduced because of the gap between the skin of the packing and the inner reactor wall, as is clear from Figure 15b.

Certain advanced packing methods were adapted for gas flow reactive experiments in order to reduce the heat transfer resistance in the gap.[14] A significant reduction of the temperature gradient was observed (Figure 16). Boger and Heibel[68] exploited the differences in thermal expansion between the aluminum monolith and the stainless steel tube in order to achieve a tight contact between the monolith and the tube wall. As a result, very high heat transfer coefficients (>1000 W/(m^2 K)) were achieved. In two-phase studies, the presence of a liquid film in the gap can alleviate the resistance to heat transfer at the wall due to the good thermal conductivity of the liquid as compared to the gas.

Two completely different concepts suggest themselves incorporating the properties of both the metallic and cordierite monoliths: metal monoliths with film flow or slug flow for

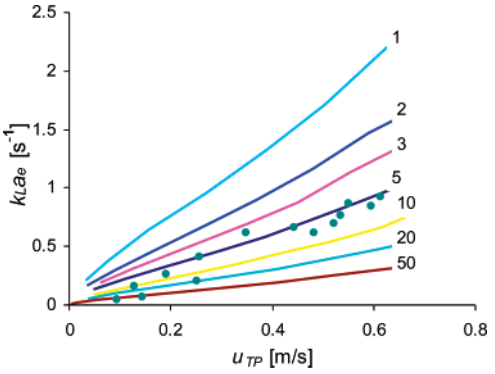

Figure 11. Mass transfer coefficient $k_L a_e$ for methane/water system as a function of the unit cell velocity u_{TP} (m/s) for a 1-m-long 200-cpsi monolith under Taylor flow conditions. The lines were calculated with the results of equation of Bercic and Pintar[59] in Table 2 using different values of the unit cell length $\Psi_{uc} = \Psi_L + \Psi_G$ from 1 mm to 30 mm. The symbols refer to oxygen experiments of physical absorption of oxygen to water using 200-cpsi monoliths.[36]

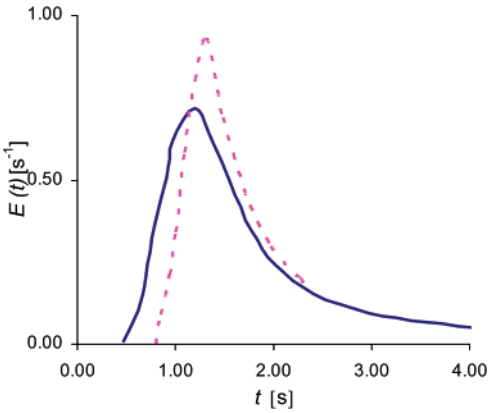

Figure 12. Exit age distribution as a function of residence time for a 25-cpsi, 500-mm-long monolith at 20 °C and 1 bar under film flow conditions, u_L = 0.023 m/s. Solid line curve represents maldistributed flow; dashed line curve represent uniformly distributed flow.[63]

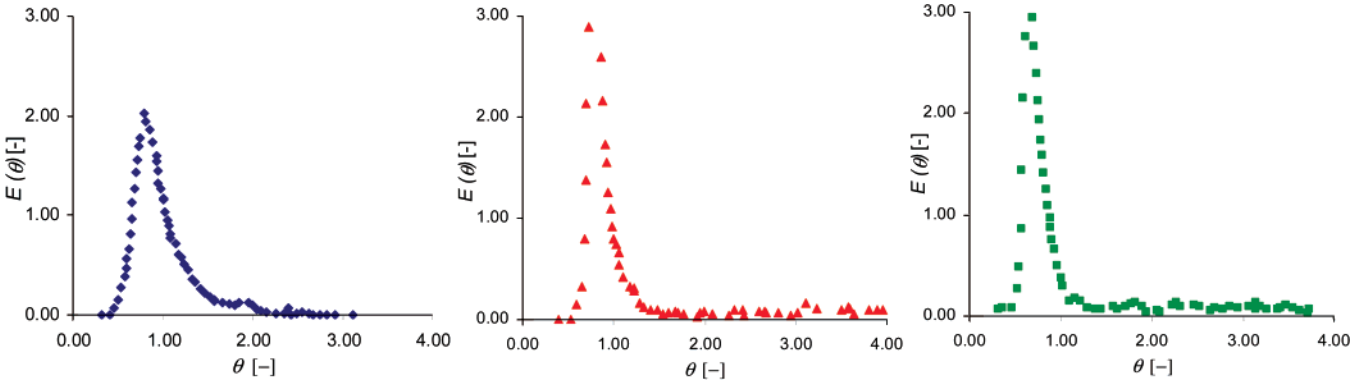

Figure 13. E curves for the three cordierite monoliths with square channels:[42] (◆) 200 cpsi, Q_L = 300 L/h, Q_G = 381 L/h; (▲) 400 cpsi, Q_L = 600 L/h, Q_G = 800 L/h; (■) 600 cpsi, Q_L = 600 L/h, Q_G = 720 L/h.

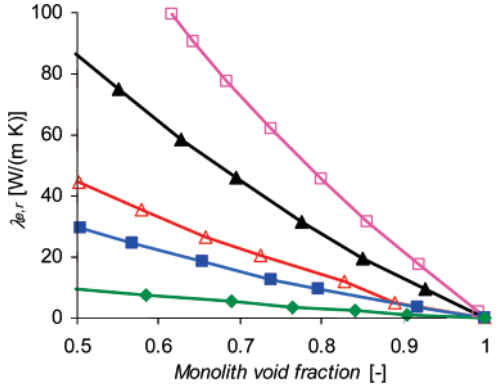

Figure 14. Effect of material properties and monolith void fraction on estimated radial effective thermal conductivity, $\lambda_{e,r}$ of honeycomb monoliths with square channels:[67] (□) Cu, (▲) Al, (△) AlN, (■) SiC, and (◆) AISI304.

efficient radial heat removal through the reactor wall, or cordierite monoliths for heat removal through convection and an external heat exchanger in an adiabatic operation. The second concept is the "monolith loop reactor" developed by Heiszwolf et al.[69] This reactor type can be applied at low conversions and high liquid flow rates, which support Taylor flow. Thus, both high mass and high heat transfer rates can be achieved. Additionally, the heat removal is decoupled from the reactor design itself, allowing independent scaling of both the reactor and the heat exchanger. De Deugd et al.[70] have presented a reactor model for the monolith loop reactor, which demonstrates a high productivity and acceptable pressure drop while ensuring a high selectivity and low-temperature rise in the reactor.

6.2. Corrugated Packings: Open Cross Flow Structure. The early corrugated packings were BX gauze packings[24] and they were used for the separation of heat-sensitive products. In the 1970s Mellapak structured packings[10] opened up a large field of applications in chemistry, petroleum chemistry, refinery, and absorption processes. Figure 17 summarizes the development history of corrugated structures since 1955.

Table 5 summarizes the typical geometric properties of the different types of corrugated packings discussed in this section.

Information on applying a catalyst support and active catalyst material on the corrugated structure is available.[11] There are numerous contributions on hydraulic and mass transfer models for corrugated packings applied in the countercurrent mode. The most important and widely applied correlations applicable for the low-interaction mode are included in this work.

Table 6 lists the experimental details of the studies on hydrodynamics, mass and heat transfer in corrugated structures along with the respective (semi-)empirical correlations.

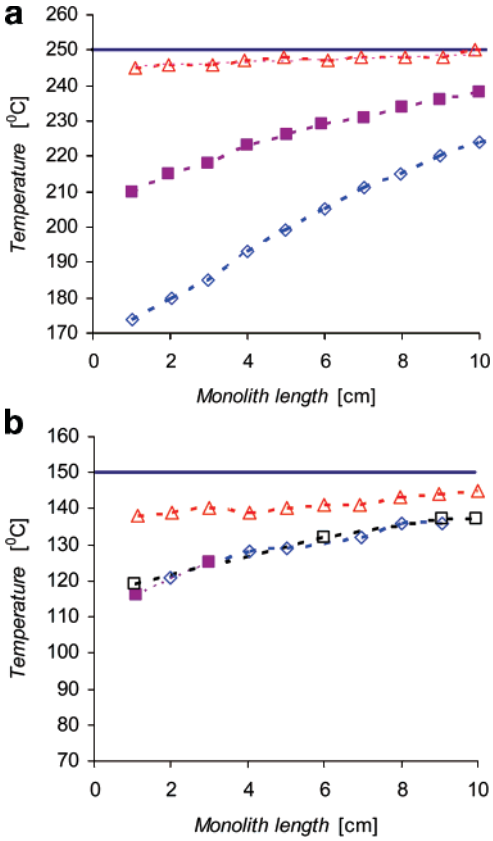

Figure 15. (a) Axial temperature profiles over a corderite monolith, T_{oven} = 250 °C, air flow rate = 10 dm^3/min (STP):[14] (—) oven temperature; (△) wall temperature; (■) peripheral temperature (close to the wall); (◇) centerline temperature. (b) Axial temperature profiles over a copper monolith, T_{oven} = 150 °C, air flow rate = 40 dm^3/min (STP).[14] (—) oven temperature; (△) wall temperature; (■) peripheral temperature (close to the wall); (□) intermediate temperature; and (◇) centerline temperature.

Because of the excellent radial mixing properties of the corrugated packings, liquid distribution is not a critical issue. Even with a poorly designed distributor, the packing redistributes the flow and hence a fully developed flow profile is achieved within a relatively short distance.

Earlier single-phase flow visualization experiments with corrugated structures similar to Katapak-M revealed three main fluid paths within such structures.[71] The first follows the orientation of the "valleys" in the corrugated sheets, which alternately transfer the fluid from one reactor wall through the structure to the opposite reactor wall in one layer, where the heat transfer occurs, and from left to the right in the neighboring

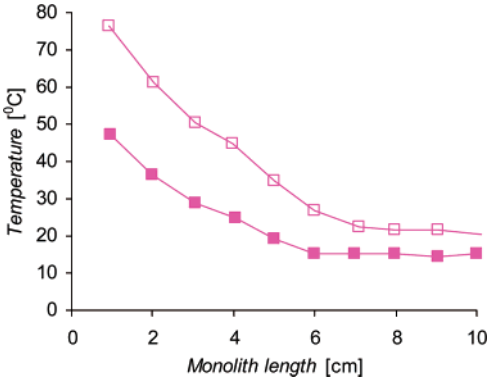

Figure 16. CO oxidation runs over copper monoliths: effect of packing of the monolith in the reactor tube on the temperature difference between monolith axis and tube wall. Flow rate = 7 dm^3/min (STP), CO_{feed} = 5 v/v%, (■) T_{oven}= 215 °C (sample with packaging), and (□) T_{oven} = 200 °C (sample without packaging).[14]

layers (see case a) Figure 18). The second main fluid path always stays inside the packing, winding itself around the cross-points of the sheet's corrugations and ensuring the good mixing behavior and the heat and mass transfer between fluid flow and structure surface (see case c) Figure 18). The third fluid path (see case b) Figure 18) is the bypassing flow in the gap between the structure and reactor wall.

Battista et al.[72] were among the first to study two phase flow patterns in corrugated structures operated in co-current mode. They trace three different flow regimes: annular flow at low liquid velocities, stratified wavy flow at higher liquid velocities and bubble flow at larger liquid velocities. They distinguish the flow regimes by measuring instantaneous current intensities as a function of time (see Figure 19). At low liquid velocities, the current intensity signal is homogeneous, at intermediate liquid velocities, irregular fluctuations in the signal are detected and at high liquid velocities, the signal becomes more homogeneous indicating that the gas−liquid flow has become more regular. The flow map of liquid velocity versus gas velocity for different liquid viscosities is given in Figure 20. The liquid velocity strongly affects the transition, while the gas flow has only a slight negative influence for all the liquid viscosities, i.e., as the gas velocity increases the transition occurs at a slightly lower liquid velocity.

For gas−liquid mass transfer, it is very important to know the surface area of the gas−liquid interface (gas−liquid interfacial area). Important results are from Brito et al.[23] who showed that the interfacial area can be significantly larger than the geometric surface area. They attribute the additional area to instabilities in the liquid flow like ripples or waves, detachment, and subsequent fragmentation of the film into liquid showers. Similar work was carried out by Frank et al.[11] (Katapak-MK) and Raynal et al.[73] (P−X packing) (see Table 6) with corrugated structures without any perforations. They observed that the ratio of interfacial area to geometric surface area increased with increasing liquid flow-rates but the ratio never went above one at comparable or even higher liquid flow-rates. The ratio of gas−liquid interfacial area to the geometric surface area obtained by Brito et al.[23] as a function of liquid Reynolds number is provided in Figure 21a and that obtained by Frank et al.[11] and Raynal et al.[73] as a function of liquid velocity is provided in Figure 21b. Clearly, the results are very different for the two types of packing. The high values Brito et al.[23] report should be restricted to Mellapak or similar packings with the corrugated plates having a rough texture in the form of perforations. These perforations add to the geometric area, which is not taken into account by the manufacturer. Second, the perforations most probably led to the formation of liquid ripples or waves adding to the effective interfacial area. Thus, the interfacial area ends up being larger than the geometric area. It is concluded that the application of the correlation for effective interfacial area developed by de Brito et al.[23] to other packings is not recommended.

Murrieta et al.[74] obtained a_e/a_p from the relationship of Shi and Mersmann[75] (see Table 6) for Sulzer-BX packing. These values can be compared with the values obtained from experimental results of Weiland et al.[76] on Montz A2 packing which is exactly the same as a Sulzer BX packing. The difference between prediction and experiment is striking (see Figure 22, parts a and b). Application of the correlation of Shi and Mersmann[75] for the prediction of the effective interfacial area in corrugated packings can be doubted. The correlation of Weiland et al.[76] is one of the few which predicts a dependence of interfacial area on gas velocity and not on liquid velocity. This indicates that the packing is wetted completely at all liquid velocities. Since the Montz A2 packing they considered is constructed of very fine stainless steel wires, it is likely that the spreading of the liquid occurs very easily and, as a consequence, the assumption of full wetting is reasonable. Furthermore, they show that the hold-up is almost independent of gas velocity until flooding occurs while the interfacial area decreases with gas velocity. This implies that liquid film thickness increases pointing to a certain degree of segregation.

Szulczewska et al.[77] performed experiments on Mellapak 250Y and observed that toluene covered the wetted surface much better than water. This effect can be attributed to the surface tension properties of the two liquids and their ability to wet metal surfaces. They observed that although toluene has better wetting properties than water, only above 0.004 m/s the total surface is covered with toluene.

Recently, liquid hold-up data was reported for corrugated open crossflow structured packings with gas−liquid flowing in co-current mode. Sidi-Boumedine and Raynal[78] demonstrated that the 1-D model of Bravo et al.[79] does not predict properly the experimental liquid hold-up because the 1-D model is based on the assumption that the packing is completely wetted which in reality is never true. The correlation (see Table 6) takes the effect of viscosity on liquid hold-up into account, but not the effect of surface tension though it is known that there is a strong effect of surface tension and contact angle on the wetting characteristics of the packing; see the study of Szulczewska et al.[77] Thus, the liquid hold-up correlation should be improved further by taking the effect of surface tension into account.

There is practically no information on pressure drop correlations for two-phase film flow in the co-current down flow mode in corrugated packings, although the concept of two-phase pressure drop is well described for counter-current mode in structured packings by Stichlmair et al.[38] The method applied by them is fundamental in nature and can be used for any packing with gas and liquid flowing in trickle mode. The approach is based on the particle model in which the gas is assumed to flow around a packing particle having a characteristic dimension and the liquid increases this dimension by its adherence to the particle surface, thereby reducing the void fraction of the bed. The model was validated for a variety of random packings and a structured packing by comparing the predicted values of the irrigated pressure drop (see Table 6) to the measurements performed by different authors on different structured and random packings.

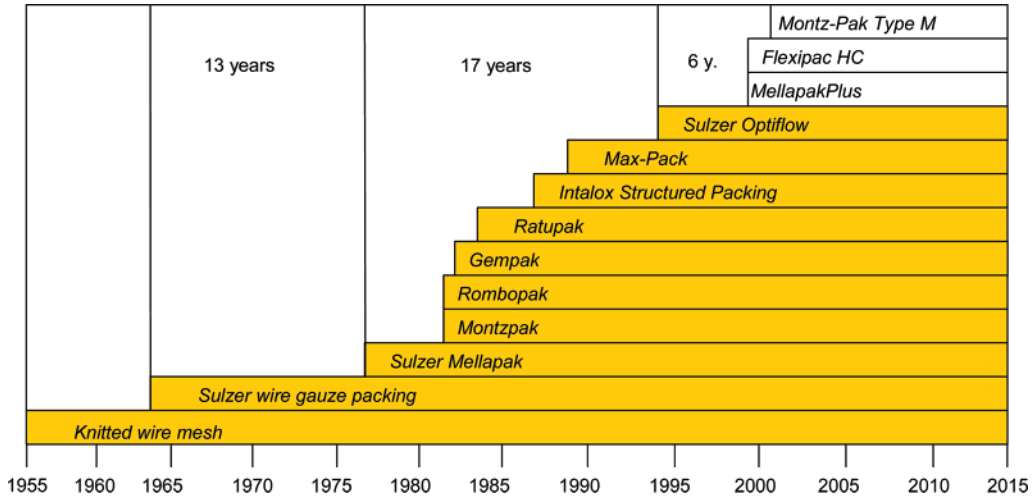

Figure 17. History of developments in structured packings. The time between major developments seems to decrease from an average of 15 years until the 1980s down to 6 years since the 1990s.[9]

Table 5. Typical Geometric Properties of Some Open Crossflow Structured Packings

no.	packing	type	surface to vol ratio (m^2/m^3)	void fraction (%)	corrugation angle (deg)	corrugation side/height (mm)	structure
1	corrugated Ni-based packing	−	820	0.88	30	5.7	layered, smooth nickel sheet packing
2	Sulzer	Mellapak					layered, sheet metal embossed and grooved
		125 Y	125	0.98	45	23	
		250 Y	250	0.96	45	11.5	
		500 Y	500	0.91	45	5.75	
3	Sulzer	Katapak-MK	650	0.85	45	4.0	layered, sheet packing
4	Montz	A2	492	0.83	60	n/a	layered, woven fabric
5	P−X	similar to Mellapak 500-X and 500-Y	446	0.93	60	8.5/6.3	layered, smooth stainless steel sheet packing
	P−Y		445	0.93	45	9.82/6.3	
6	Gempak	2B	492	0.83	n/a	11.0	layered, slit, and perforated sheet
7	Flexipac	2	233	0.95	45	18.0	layered, fluted surface and large holes
8	Sulzer	BX-packing	492	0.90	60	8.9/6.4	layered, perforated gauze
9	Flexeramic	28	282	0.70	45	9.0	layered, ceramic packing
10	Katapak-S	270	270	0.46	45	$d_h = 6.9$	wire gauze corrugated sheets forming
		440	440	0.6	45	$d_h = 5.4$	channels filled with solid catalyst
11	Montz Multipak	I	355	0.56	60	$d_h = 6.3$	corrugated sheets and flat envelopes of wire gauze containing the catalyst
		II	325	0.575	60	$d_h = 7.0$	

All models for predicting the mass-transfer rates of corrugated packings are based on experimental results for distillation systems. Although such systems involve transfer resistances on both vapor and liquid sides, it has usually been assumed that the vapor side dominates and thus models for the liquid side do not need high precision.[74] Bravo et al.[79] proposed the first general model for predicting the mass transfer performance of wire gauze structured packings. The liquid-side mass transfer coefficient was estimated from the penetration theory (see Table 6). The model was validated by various authors.[74,80,81] Raynal et al.[73] used the penetration theory to validate their experimental data but found that the model resulted in an important underestimation of the liquid side mass transfer coefficient, k_L. They assumed that the characteristic dimension of the packing, S (channel side of the packing), is appropriate for the gas flow since it occupies most of the volume, but this is not the case for the liquid flow which is of trickling type. By choosing 4δ as the characteristic length, they found excellent agreement between their experimental values and the model.

Brunazzi and Paglianti[82] developed a Sherwood correlation as a function of packing height in terms of Graetz number and mixing effects in corrugated inclined plates in terms of the Kapitsa number (see Table 6). In contrast with the other authors they took into account the effect of column height on the mass transfer performance of a corrugated packing. They claim from their experimental data that there is a critical packing height below which the liquid side mass transfer is a function of packing height. They compared their model with the model proposed by Bravo et al.[83] and found that their model successfully fitted the experimental data of Mellapak 250-Y and Sulzer-BX (see Figure 23). They used a mechanistic model of Brunazzi et al.[84] to estimate the interfacial area for mass transfer (see Table 6). Note that the correlation of Brunazzi and Paglianti[82] is of a general type and can be used to predict the performances of columns equipped with completely different kinds of structured packing. Mellapak type has an embossed and grooved surface whereas BX type is made of perforated gauze. As seen in Table 6, only the constants in the correlation would take a different value if used for different structured packing.

Two studies on determination of $k_L a_e$ and a_e for corrugated packings in a co-current downflow operation have been reported. The results are presented in Table 7. They can be directly

Table 6. Correlations for Hydrodynamic and Transport Parameters for Open Crossflow Structured Packings

reference	correlations	method	geometric properties	operating conditions	comments
Battista et al.[72]	flow transition−film flow to pulse flow no correlation available	current intensity, using a polarized electrode, effect of viscosity: 0.6−1.1% cmc	corrugated smooth nickel sheets, 40 mm × 40 mm × 350 mm[1]	co-current down flow $\mu_L = 0.001-0.073$ m/s $\mu_G = 0-0.35$ m/s	effect of viscosity studied
de Brito et al.[23]	gas−liquid interfacial area in film flow $(a_e/a_p) = 0.465 Re_L^{0.3}$	lean CO_2 absorption with reaction in aqueous NaOH	Mellapak 125-Y, 250-Y, 500-Y, 295 mm i.d. × 420 mm long[2]	co-current down flow $u_L = 0.005-0.02$ m/s $u_G = 0.4-2.8$ m/s	$a_e \propto u_L^{0.3}$
Frank et al.[11]	gas−liquid interfacial area in film flow $a_e = 95L^{0.4}$	lean CO_2 absorption with reaction in aqueous diethanolamine	Sulzer Katapak-MK FeCr-alloy 38 mm i.d. × 100−500 mm long[4]	co-current down flow $u_L = 0.002-0.01$ m/s $u_G = 0.01-0.1$ m/s	$a_e \propto u_L^{0.4}$
Raynal et al.[73]	gas−liquid interfacial area in film flow no correlation available	lean CO_2 absorption with reaction in $NaOH/NaHCO_3$	P−X 54 mm i.d. × 2 m long[5]	co-current down flow $u_L = 0.01-0.1$ m/s $u_G = 1.4$ m/s	$a_e \propto u_L$ up to $u_L = 0.04$ m/s and then independent indicating all all geometric surface area is wetted
Weiland et al.[76]	gas−liquid interfacial area in film flow $a_e = 265(\mu_G \rho_G^{1/2})^{-0.4}$	lean CO_2 absorption with chemical reaction in aqueous NaOH	MontzA2 1.06 m long, 0.15 m i.d.[3]	co-current down flow $u_L = 0.0028-0.011$ m/s $u_G = 0.46-1.0$ m/s	dependence on gas velocity found
Sidi-Boumedine et al.[78]	liquid hold-up in film flow $\beta_L = \beta_{w0}\left(\frac{\mu_L}{\mu_w}\right)^{1/3} + K\frac{T}{\rho_L}\left(\frac{\mu_L}{\mu_w}\right)^{1/3}$, $T = \rho_L Q_L \frac{Bh}{4S}$	mapping the liquid holdup across the packing with γ-ray tomographic measurements	P−X and P−Y 400 mm i.d. × 2 m long[5]	co-current down flow $u_L = 0.006-0.057$ m/s $u_G = 0.1$ m/s	effect of viscosity studied $\beta_L \propto (m_L/\mu_w)^{1/3}$
Stichlmair et al.[38]	pressure drop in film flow $\frac{\left(-\frac{dp}{dz}\right)_{irrigated}}{\left(-\frac{dp}{dz}\right)_{dry}} = [1-\epsilon(1-\beta_L/\epsilon)]^{-4.65}\left[\frac{1-\epsilon(1-\beta_L/\epsilon)}{1-\epsilon}\right]^{(2+c)/3}$, $\beta_L = 0.55 Fr_L^{1/3}$ $Fr = u_L^2 a_P/g\epsilon^{4.65}$	phenomenological model based on the fluidized bed analogy, validated packings in countercurrent flow below the load point	Mellapak 250-Y plastic,[2] data from Sulzer used for validation	countercurrent $u_L = 0-0.041$ m/s $u_G = 0.5-4$ m/s	$\beta_L \propto u_L^{1/3}$
Bravo et al.[85]	pressure drop in film flow $\left(-\frac{dp}{dz}\right)_{dry} = \frac{3}{4} f \frac{(1-\epsilon)}{\epsilon^{4.65}} \frac{\rho_G \cdot u_G^2}{d_h}$, $f = \frac{c_1}{Re_g} + \frac{c_2}{Re_g^{1/2}} + c_3$ $c = \frac{1}{f}\left[\frac{c_1}{Re_g} + \frac{1}{2}\frac{c_2}{Re_g^{1/2}}\right]$	based on the channel model, validated for structured packings in countercurrent flow below the load point, i.e., film flow regime	Gempak[6] and Flexipac[7] pressure drop data from Koch used for validation	countercurrent $u_L = 0-0.05$ m/s $u_G = 0-0.15$ m/s	$\beta_L \propto u_L^{0.36}$ validated for aqueous and organic systems
Rocha et al.[86]	pressure drop in film flow $\left(-\frac{dp}{dz}\right)_{dry} = \frac{f\rho_G u_{G,eff}^2}{d_h}$, $f = c_1 + \frac{c_2}{Re_g}$, $u_{G,eff} = \frac{u_G}{\epsilon(1-\beta_L)\sin\theta}$ $\left(-\frac{dp}{dz}\right)_{dry} = \frac{A\rho_G}{d_h\epsilon(1-\beta_L)\sin\theta} u_G^2 + \frac{\beta\rho_G}{d_h^2\epsilon(1-\beta_L)\sin\theta} u_G$ packing-geometry-dependent constants	based on the channel model, validated for structured packings in countercurrent flow below the load point	Flexipac,[7] Gempak,[6] Sulzer BX,[8] column i.d. 430 mm and height 3 m	countercurrent $u_L = 0-0.035$ m/s $u_G = 0-0.5$ m/s	takes into account the effect of gas and liquid flow rates on liquid holdup, hold-up and pressure drop model validated for air−water system, pressure drop model also validated at high pressure and low surface tension liquids

Table 6. (Continued)

reference	correlations	method	geometric properties	operating conditions	comments
Uresti-Melendez et al.[87]	pressure drop in film flow $\frac{\left(-\frac{dp}{dz}\right)_{irrigated}}{\left(-\frac{dp}{dz}\right)_{dry}} = \frac{1}{(1 - C\beta_L)^5}$, $C = 0.626 + 32.669s$, $C\beta_L = 2.5113 {Fr_L}^{0.36}$ $\beta_L = \left(4\frac{F_t}{S}\right)^{2/3} \frac{3\mu_L u_L}{\rho_L(\sin\theta)\epsilon g_{eff}}$ $F_t = \frac{a_e}{a_P} = \frac{29.12(We \times Fr)_L^{0.15} S^{0.359}}{Re_L^{0.2}\epsilon^{0.6}(1 - 0.93\cos\gamma)(\sin\theta)^{0.3}}$ efficiency of Shi and Mersmann[75] θ = angle with respect to horizontal axis $C\beta_L = 0.381 {Fr_L}^{0376} {Re_{G,eff}}^{0.257}$, $Re_{G,eff} = \frac{u_{G,eff} S \rho_G}{\mu_G}$	based on the channel model, validated for structured packings in countercurrent flow below the load point, i.e., film flow regime	pressure drop measurements from databank for Flexeramic[9] packings using air−water system	countercurrent $u_L = 0-0.035$ m/s $u_G = 0.5-4.5$ m/s	takes into account the effect of gas and liquid flow rates on liquid holdup
Frank et al.[11]	gas−liquid mass transfer in film flow $k_L a_e = 0.0025 u_L \rho_L$	lean CO_2 absorption with reaction in aqueous triethanolamine desorption of oxygen from saturated water into nitrogen desorption of CO_2 from water into air and absorption of chlorinated solvents	Sulzer Katapak-MK FeCr-alloy 38 mm i.d. × 100−500 mm long[4]	co-current down flow $u_L = 0.002-0.01$ m/s $u_G = 0.01-0.1$ m/s co-current down flow $u_L = 0.005-0.02$ m/s $u_G = 0.4-2.8$ m/s	$k_L \propto {u_L}^{0.6}$
Laso et al.[10]	gas−liquid mass transfer in film flow $k_L a_e = 0.574 {u_L}^{0.62}$ Mellapak 250-Y $k_L a_e = 0.713 {u_L}^{0.71}$ Mellapak 500-Y		Mellapak 125-Y, 250-Y, 500-Y, 295 mm i.d. × 420 mm long[2]		
Brunazzi et al.[82]	gas−liquid mass transfer in film flow $Sh_L = A\frac{Gz^B}{Ka^C}$, $Sh_L = \frac{k^L 4\delta}{D_L}$, $Ka = \frac{{\sigma_L}^3 \rho_L}{{\mu_L}^4 g}$, $Gz = Re_L Sc_L \frac{\delta}{H}$ $H = \frac{Z}{\sin a}$, $\delta = \left(\frac{3\mu_L}{\rho_L g \sin a}\frac{u_L}{\beta_L \sin a}\right)^{0.5}$ $\frac{a_e}{a_p} = \left(\frac{d_h \sin\theta}{4\epsilon}\right){\beta_L}^{1.5}\left(\frac{\rho_L g}{3\mu_L u_L}\right)^{0.5}$ $A = 16.43$, $B = 0.915$, $C = 0.09$ for Mellapak 250-Y (metal/plastic) $A = 63.1$, $B = 0.676$, $C = 0.09$ for Sulzer BX (plastic) $\frac{a_e}{a_p} = \left(\frac{d_h \sin\theta}{4\epsilon}\right){\beta_L}^{1.5}\left(\frac{\rho_L g}{3\mu_L u_L}\right)^{0.5}$		Mellapak 250-Y, 100 mm i.d. × 0.4−2 m long[2]		validated the model by using distillation data using Sulzer-BX packing also validated for liquids of different surface tension and viscosities

Table 6. (Continued)

reference	correlations	method	geometric properties	operating conditions	comments
Brunazzi et al.[84]	gas−liquid mass transfer in film flow $u_{L,eff} = \left(\frac{3\Gamma}{2\rho_L}\right)\left(\frac{\rho_L{}^2}{3\mu_L\Gamma}\right)^{1/3}$ (falling film relationship) or $k_L = 2\left(\sqrt{\frac{D_L}{\pi t}}\right)$ or $k_L = 2\left(\sqrt{\frac{D_L u_{L,eff}}{\pi s}}\right)$ $u_{L,eff} = \frac{u_L}{\epsilon\beta_L \sin\theta}$			countercurrent $u_L = 0-0.008$ m/s $u_G = 0.4-1.4$ m/s	
Bravo et al.[79]	gas−liquid interfacial area calculated using the following correlation from Shi and Mersmann[75] $\frac{a_e}{a_p} = \frac{29.12(We \times Fr)_L{}^{0.15} s^{0.359}}{Re_L{}^{0.2}\epsilon^{0.6}(1 - 0.93\cos\gamma)(\sin\theta)^{0.3}}$, γ = contact angle for surface material wettability				modeling work using penetration theory
Battista and Bohm[88]	wetted area for liquid−solid mass transfer $(a_{LS}/a_p) = 0.58 Re_L{}^{0.5} Fr_L{}^{0.1}$ $Re_L < 5$ $(a_{LS}/a_p) = 0.85 C Re_L{}^{0.25} Fr_L{}^{0.1}$ $Re_L \geq 5$	adding red ink to the circulating liquid and measuring the colored area	corrugated packing made of smooth nickel sheets, 40 mm × 40 mm × 500 mm long[1]	co-current down flow $u_L = 0.01-0.065$ m/s $u_G = 0.0-0.3$ m/s	measured values compared to those predicted by the correlations of Billet
Battista and Bohm[88]	liquid−solid mass transfer coeff $Sh(a_{LS}/a_p) = 0.33 Sc^{1/3} Re_L{}^{0.63}$ $1256 < Sc < 17045$, $0.15 < Re_L < 84$	electrochemical technique	corrugated packing made of smooth nickel sheets, 40 mm × 40 mm × 500 mm long[1]		verified for different liquid viscosities $a_e/a_p \propto 1/\mu_L$
Macias-Salinas et al.[89]	residence time distribution for gas phase $Pe_G = 4.2468 \times 10^8 Re_g{}^{-0.896} \times 10^{-0.00208 Re (d_e a_p)^{-7.792}}$ residence time distribution for liquid phase $Pe_L = 8.154 F_i{}^{0.7082} (3/\sin^2\phi)^{1.159} (d_e a_p)^{6.337}$ $381 < Re_g < 3516$, $25 < Re_l < 122$, $45° < \phi < 60°$, $F_i = \mu u / d_{eq}{}^2 \rho g$, $1.5 \times 10^{-6} < F_i < 1.59 \times 10^{-5}$, $3.16 < d_e a_p < 3.53$	dynamic response conductivity measurement technique, air/water system, helium as tracer for gas phase and NaCl as tracer for liquid phase	column of 4.3 mm i.d. and 2.1 m long packed with Flexipac-2[7] and Sulzer-BX[8]	counter-current $u_L = 0.03-0.09$ m/s $u_G = 0.75-2.5$ m/s	evaluated effect of axial mixing on mass transfer processes Sulzer BX with lower axial mixing in both phases than Flexipac-2
Kolodziej et al.[90]	residence time distribution for liquid phase Multipak-II $D_{ax,L} = 0.0663 u_{L,eff}$ Katapak-S-440 $D_{ax,L} = 0.0332 u_{L,eff}$	dynamic response technique nitrogen/ *n*-heptane system with *o*-xylene as tracer	Katapak-S-270;[10] 440 Multipak I and II[11] 55 mm diameter × 1.9 m long	counter-current $u_L = 0.001-0.008$ m/s $u_G = 0.0-1.6$ m/s	validated for a lower surface tension liquid, Multipak shows higher axial dispersion than Katapak-S
von Scala et al.[71]	effective radial thermal conductivity, wall heat transfer coefficient no correlation developed heat transfer parameters $\lambda_{e,r}$ and a_w evaluated based on a two-dimensional pseudohomogeneous steady-state plug flow model	heating of cool air and measuring the radial temp profile at the exit of the tube filled with the packing	Katapak-M packing, 48-mm-diameter packed in 50 mm i.d. × 400 mm long	$u_G = 0.5-1.5$ m/s	good agreement between CFD simulations and experimental results

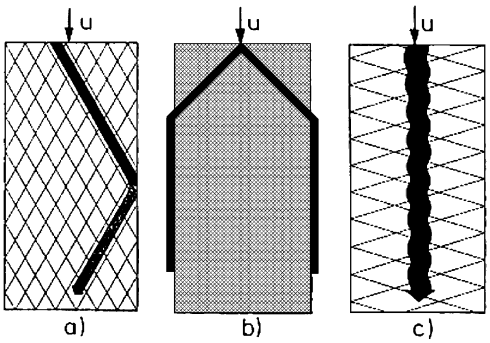

Figure 18. Main fluid paths in open crossflow structures: (a) flow following the valleys, which is reflected at the side wall and returns through a valley of the opposite plate; (b) bypassing flow in the gap between the structure and reactor wall; (c) fluid following the main flow direction and crossing the valleys. Adapted from ref 71.

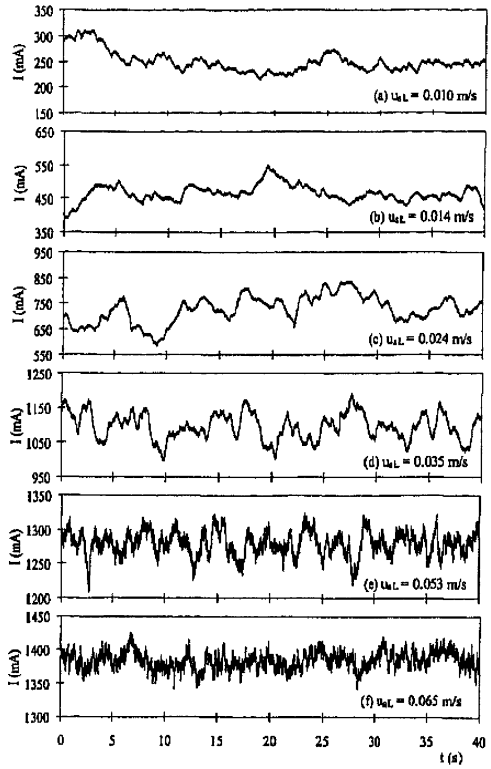

Figure 19. Flow regime transitions in OCFS packing made of smooth nickel sheets are identified from the time series of instantaneous current intensities for the nitrogen/potassium ferrocyanide and ferricyanide aqueous solutions at the following gas and liquid velocities: $u_G = 0.24$ m/s and (a) $u_L = 0.01$ m/s; (b) $u_L = 0.014$ m/s; (c) $u_L = 0.024$ m/s; (d) $u_L = 0.035$ m/s; (e) $u_L = 0.053$ m/s; (f) $u_L = 0.065$ m/s. The film flow regime corresponds to low or no current intensity fluctuations, stratified wavy flow to significant current intensity fluctuations.[72]

compared as the corrugated packings used by both authors have almost the same geometric dimensions, including the column diameter. Raynal et al.[73] found $k_L a_e$ and a_e values which are higher than those obtained by Frank et al.[11] The measurements were carried out at different velocities and, as a consequence, the flow regime might have been different in both cases. We expect that the measurements of Frank et al.[11] were carried out in trickling flow regime (low interaction) and that of Raynal et al.[73] were carried out either in Taylor or churned flow (high interaction).

The fractional surface wetting measured by Battista and Bohm[88] is plotted at different liquid viscosities against the liquid velocity in Figure 24. From the values it is clear that problem

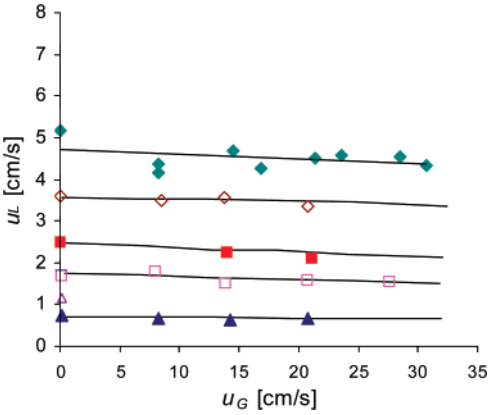

Figure 20. Flow map of film flow to stratified wavy flow in OCFS packing made of smooth Nickel sheets at different liquid viscosities: (◆) μ_L = 0.97 mPa s; (◇) μ_L = 1.17 mPa s; (▲) μ_L = 4.4 mPa s; (△) μ_L = 7.4 mPa s; (□) μ_L = 10.0 mPa s; (■) μ_L = 12.6 mPa s.[72]

of channeling at low liquid flow rates and incomplete wetting over the complete range of liquid velocity studied persist. Not surprisingly, viscosity shows a negative effect on the fractional surface wetting.

Macias-Salinas et al.[89] evaluated the impact of axial mixing on mass transfer efficiency based on mass transfer data reported for the cases of gas absorption, stripping, water cooling and distillation using Flexipac-2 and Sulzer-BX packing. They concluded that neglecting axial mixing can lead to an overestimation of the mass-transfer driving forces, thus leading to an underestimation of the mass transfer coefficients. Results of oxygen desorption from water into air showed that deviation from plug flow diminished as liquid flow increased. This case clearly demonstrated the importance of properly assessing the impact of axial mixing effects in order to be able to establish the range of operating conditions over which these effects can be safely neglected.

Only one paper reports gas phase heat transfer measurements in Katapak-M packing.[71] The heat transfer parameters $\lambda_{e,r}$ and α_w increase with increasing flow rate due to (a) improved mixing inside the structure and (b) reduced thickness of the boundary layers. The influence of the gap (1−2 mm) between the structure and the wall on the heat transfer rate was also studied. With increasing gap, the bypass flow becomes more important and mixing is less efficient, decreasing the overall heat transfer coefficient. Effective radial thermal conductivities, $\lambda_{e,r}$, were found to be between 1 and 2 W/(m K) and the wall heat transfer coefficients, α_w, were between 60 and 80 W/(m^2 K). These values are very low compared to what are actually required in multiphase exothermic reactions. In two-phase flow, the liquid hold-up in addition to the mass flow-rate and the heat capacity plays a prominent role in the heat transport mechanism. Additionally, the turbulence generated by the interaction between the gas and liquid intensifies radial mixing giving rise to relatively high $\lambda_{e,r}$. The intense radial mixing directed from the packing to the wall also might lead to convective transport of heat at the wall and thus a relatively high α_w. This hypothesis should be further investigated.

6.3. Corrugated Packings: Closed Cross Flow Structures. The closed crossflow structure is also made of thin corrugated metal sheets arranged side by side with opposing channel orientations but in addition a flat sheet is inserted between the corrugated sheets (Figure 25). The open channel packing geometry is then transformed into a monolith-like structure with a multiplicity of closed inclined triangular channels. This

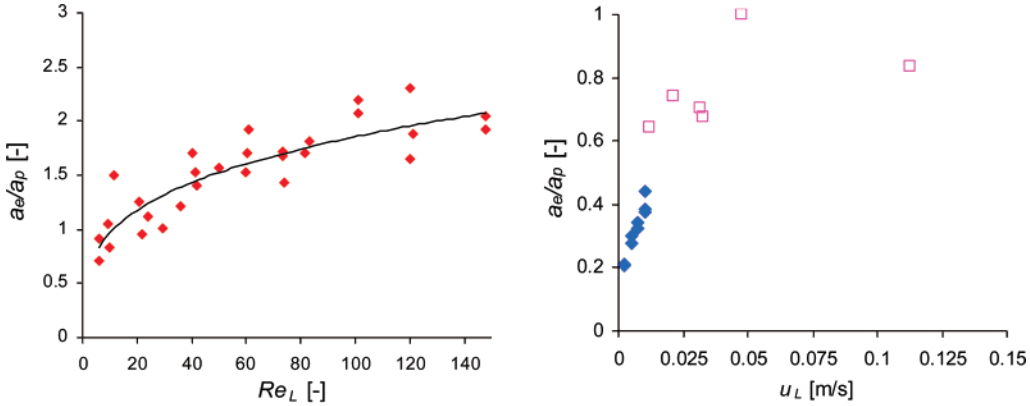

Figure 21. Ratio of gas−liquid interfacial area to geometric surface area, a_e/a_p, in open crossflow structures as a function of the Reynolds number: (a) left graph, Mellapak packing;[23] (b) right graph, (◆) Katapak-M packing[11] and (□) P−X packing[73] (similar to Mellapak 500-X without perforations).

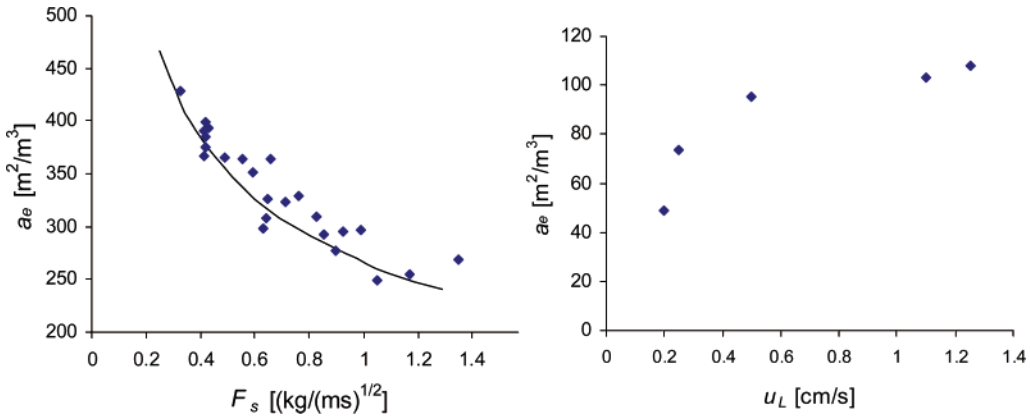

Figure 22. Comparison between (a) left graph, experimental results of effective interfacial area, a_e (m^2/m^3) of Montz A2 packing,[76] and (b) right graph, values obtained for the effective interfacial area from the correlation of Shi and Mersmann[75] for a Sulzer BX packing at $Fs = 1.18$ (m/s)(kg/m^3)$^{0.5}$.

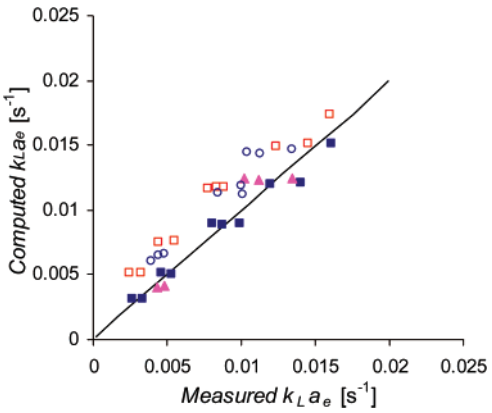

Figure 23. Parity plot of k_La_e, comparison between experimental and predicted values obtained by using the model of Brunazzi et al.[82] and the model proposed by Bravo et al.[83] for Sulzer BX plastic (□, Bravo et al.; ■, Brunazzi et al.) and BX metal packing (○, Bravo et al.; ▲, Brunazzi et al.). Experimental k_La_e values obtained with air/CO_2/water system.

way the specific surface area can be increased considerably.[91] Wash coating of closed crossflow structured packings can be carried out in the same manner as open crossflow structured packings.

Initial flow distribution in closed channel packings is as important as it is for monoliths, since there is no exchange of liquid between adjacent channels.

Flow patterns in the closed channels are similar to those in a monolith as the channels are closed with no interconnection with adjacent channels. Thus, radial mixing will be very limited. What makes this structure so special is that it is open at the wall and as the flow is directed from left to right and vice versa in the adjacent layers it directly hits the reactor tube wall causing disturbances of the stagnant layers at the wall.[25] If the channel size is sufficiently small, Taylor flow will be induced, provided the ratio gas to liquid flow rate is in the right range. In combination with improved heat transfer at comparatively lower pressure drop, Taylor flow might result in high mass transfer rates.

Closed channel packings with larger channels ($d_h = 11.3$ mm) were studied by Behrens et al.[91] for counter-current applications. They concluded that because of the inclination of closed channels, the liquid tends to flow in rivulet form along the base of channel formed between corrugations and the flat plate, which implies a significant loss of effective surface area, and hence an increased bypassing. This phenomenon might not occur in smaller diameter channels as due to significant surface tension forces and capillary action wetting will be high.

The pressure drop in closed channel packing is lower than the standard packing even though the closed channel has a higher geometric surface area.[91] By inserting a flat sheet between two corrugated sheets the energy consuming gas−gas interaction is replaced with less energy consuming gas−liquid friction.

Although pressure drop correlations are not found in literature for closed channel packings, the two-phase pressure drop can be modeled as a function of dry pressure drop and liquid hold-up, similar to the corrugated packing.

The closed channel packings being open at the wall, very efficiently help in disturbing the laminar film present in the gap between the skin of the packing and the wall when the flow is

Table 7. k_La_e and a_e Values Obtained in Open Crossflow Structures

author	range of gas and liquid velocities	flow regime	k_La_e (s^{-1})	a_e (m^{-1})
Frank et al.[11]	$\mu_L = 0.002-0.01$ m/s $\mu_G = 0.01-0.1$ m/s	low interaction	0.005−0.025	150−250
Raynal et al.[73]	$\mu_L = 0.01-0.1$ m/s $\mu_G = 1.4$ m/s	high interaction	0.15−0.25	200−500

Table 8. Typical Geometric Properties of Commercially Available Knitted Wire Packing

packing	supplier	surface-to-volume ratio (m^2/m^3)	void fraction (%)	wire diameter (μm)	crimp pitch (mm)
Goodloe	Koch-Glitsch	1920	0.95	114	8.0
HYFlux	Evergreen Tech. Pvt. Ltd.	1932	0.95	~100	~8.0

directed from the structure to the wall. This creates turbulence thus improving the heat transfer from the packing to the wall. Unlike the monolith, the closed channel packing shows a lower sensitivity to gap sizes between the skin of the packing and the wall.[25] Flow visualization experiments carried out by Schildhauer[25] have confirmed that the flat plate between the corrugated sheets directs the fluid more efficiently toward the inside reactor wall to improve overall heat transfer coefficients.

Single phase heat transfer measurements with closed channel packings show improved wall heat transfer coefficient at lower pressure drop compared to open crossflow structured packing or a bed of spherical particles.[25]

6.4. Knitted Wire Structured Packing. Knitted wire is a family of structured tower packings, which are particularly useful in distillation applications when a moderate to large number of theoretical stages have to be accommodated in a limited height of the tower. This packing is originally named as Goodloe packing with the essential feature devised by A. M. Goodloe of the Metal Textile Corp.[92]

This packing is characterized by bundles of knitted strands of stainless steel wires. The knitted strands are flattened, crimped, and rolled to give the desired diameter of the cylindrical packing.[93] It gives a combination of low-pressure drop and excellent wetting characteristics with a low surface tension liquid.

The inherent capillary action of the fine wires causes the liquid to spread into thin films that continuously combine and divide for optimum mixing and contact with the gas throughout the entire packing volume. The net result is a packing with high mass transfer efficiency and low-pressure drop. Both co-current and counter-current (pre-flooding) data are available in the literature. Unfortunately, there is no data or information on the heat transfer properties and catalytic coating methods for this packing as it is primarily used in distillation processes.

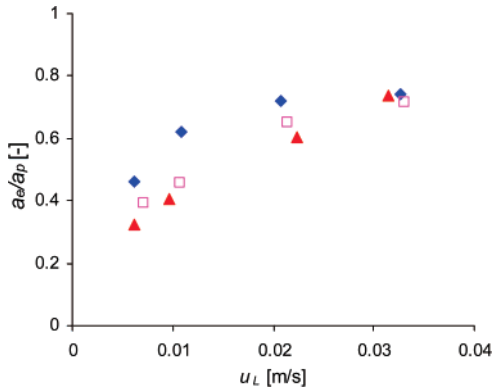

Figure 24. Fractional surface wetting for OCFS packing made of smooth nickel sheets, a_e/a_p, as a function of μ_L for different liquid viscosities: (◆) $\mu_L = 1.0$ mPa s, (□) $\mu_L = 3.0$ mPa s, and (▲) $\mu_L = 5.0$ mPa s.[88]

Table 8 gives typical geometric properties of these packings

Table 9 lists the experimental details of the studies on hydrodynamics and mass transfer in knitted structured packing along with the respective empirical correlations.

Unlike the corrugated packings, this packing has almost no self-distribution property.[26] Similar to monoliths, the liquid distributor design plays a crucial role in the performance of reactors packed with such packings.

Figure 26 presents a flow map for the knitted wire packing, showing the transition from trickle flow to pulse flow, pulse flow to slug or Taylor flow and slug flow to spray flow. The fitted correlation (see Table 9) (for original data see Patil and Sharma[94]) is obtained by regressing the experimental data. The correlations have not been tested for other systems apart from air and water, making their applicability limited. Note that the transition from one to another regime is quite sharp. Since the data was obtained by ocular inspection it is likely that a transition region could not be detected.

Patil and Sharma,[94] Weiland et al.,[76] and Niranjan et al.[93] measured gas−liquid interfacial areas in the low interaction regime for this packing. The results are presented in Table 10.

Parts a−c of Figure 27 show the gas−liquid interfacial area as a function of gas and liquid velocities measured by the three authors. The interfacial areas are in the same range but the dependences on the gas and liquid velocities vary significantly. Since the interfacial areas measured are significantly smaller than the geometric area of the packing and the dependence on the gas velocity is weak, the differences observed might be due to experimental errors and hence the correlations can be questioned. The high a_e values observed by Niranjan et al.[93] at relatively low liquid and gas velocities are remarkable. Since the measurements carried out by them are in counter-current gas−liquid mode, it is concluded that the mode of operation has a significant effect on the hydrodynamics and eventually the interfacial area. Patil and Sharma[94] also investigated the effect of surface tension on the effective interfacial area by adding 5 vol % 2-propanol in aqueous sodium dithionite. As expected, the interfacial area was higher than for the aqueous system. The increase in a_e was observed to be different in different flow regimes and it was approximately 15%−20%, 30%−45%, and 80%−125% for trickle, pulse and slug flow regime, respectively. In the case of slug flow, they observed foaming with values of a_e as high as 2470 m^2/m^3, which is higher than the geometric surface area of the packing. This result is not surprising as the high values of a_e in the slug flow might arise due to the formation and breaking of foaming slugs, analogously to the results obtained by de Brito et al.,[23] which was already elaborated upon in section 6.2. Thus, Patil and Sharma[94] successfully demonstrated that the surface tension has a significant effect on the effective interfacial area.

Summarizing, the wetting characteristics of this packing is are remarkably good for low surface tension liquids. Though

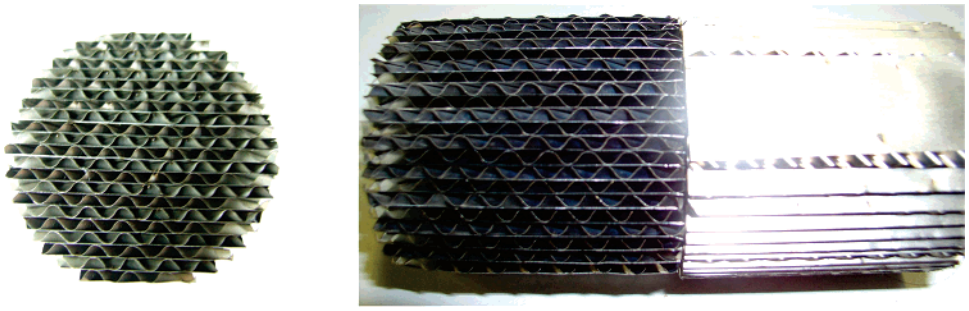

Figure 25. (a) Right photo: top view of CCFS. (b) Left photo: side view of two CCFS elements rotated by 90° to each other.

these packings have high geometric surface areas, there is yet no know-how on how to coat these packings with catalytic material in order to achieve considerable mechanical strength and activity. It should be realized that these packings are formed out of thin woven fibers, and it can be speculated that coating the packing would destroy the geometric surface area created by the woven fibers. This would mean that after coating the area available for mass transfer and reaction might be considerably lower than stated by the manufacturer.

The pressure drop model developed by Patil and Sharma[94] is not based on any mechanistic model (Table 9) as it is only fitted against experimental data. The two-phase pressure drop is not a simple addendum to the single-phase pressure drop but it is higher due to the formation of a liquid film on the filaments thus lowering the effective diameter of the channels for the gas flow. The channel model developed by Bravo et al.[85] and Rocha et al.[86] for countercurrent flow in corrugated packings is also recommended for these packings in the trickle flow regime.

The $k_L a_e$ values measured by Niranjan et al.[93] and Weiland et al.[76] are compared in Table 10. Again the dependence on gas and liquid velocities are different in both cases. The countercurrent mode of operation applied by Niranjan et al.[93] has a significant effect on hydrodynamics and eventually the volumetric gas to liquid mass transfer coefficient which includes the interfacial area.

6.5. Foams: Metals-, Ceramic-, and Graphite-Based. Solid foam packings represent a generation of materials combining high specific surface area with low-pressure drop. This is largely due to the open-celled structure with high voidages (up to 97%) of small dimensions. Solid foams are produced in a variety of materials (metal, ceramics, carbon, SiC, polymers, etc.). Metallic foams have in recent years seen increased application for flow control and heat transfer enhancement.[95] The excellent performance of metallic foams in these applications is attributed to their intricate interfacial geometries, creating a highly tortuous flow path with a continuous disruption of established hydrodynamic and thermal boundary layers. In the case of aluminum foam, good thermal contact achieved with the foam brazed onto an aluminum substrate material is combined with the good thermal conductivity of aluminum.[95] The review by Banhart et al.[19] outlines the methods and procedures for producing these and many other types of foam.

The applications considered for these foam materials in the chemical industry have been minimal. Only single phase studies have been reported, in ceramic foams on mass and heat transfer rates by Richardson et al.,[96] pressure drop in aluminum foams by Fourie and Du Plessis,[95] axial dispersion in nickel foams by Montillet et al.,[97] heat transfer characterization by Gianni et al.,[98] and mass transfer characterization by Gianni et al.[99] in Fecralloy and copper foams. Recently characterization of foams with respect to pressure drop and liquid hold-up for countercurrent operation was reported by Stemmet et al.[100] and gas to liquid mass transfer, pressure drop, liquid hold-up and RTD were reported by Stemmet et al.[101] for co-current up flow operations. Washcoating of the Fecralloy foam with a stable layer of Pd/γ Al_2O_3 is reported in the literature.[99]

Table 11 lists the experimental details of the studies on hydrodynamics and mass transfer in foams along with the respective empirical correlations.

The two-phase pressure drop in foams can be modeled in a similar way, i.e., as a function of the dry pressure drop and liquid hold-up. The dry pressure drop concept in foams is well-defined[95,102] and was modeled based on the Forchheimer equation.[103] This relationship is synonymous with the Ergun model,[104] in which the pressure drop is the sum of viscous and inertial terms.

Stemmet et al.[100] measured pressure drop in the liquid phase in countercurrent mode for a 2-D open-celled solid aluminum foam in the range of 5−40 PPI with voidages of 92%−94%. Figure 28 presents the dry and wet pressure drop versus gas load for different PPI and liquid velocities. Pressure drop increases not only with increasing gas loads but also with increasing PPI and liquid velocity. This plot can give an indication of the pressure drop in a co-current operation with a fair assumption that the low interaction regime in counter-current mode will render similar pressure drops as in co-current low interaction regime.

As given in Table 11, Stemmet et al.[105] used the relative permeability model to predict the total liquid hold-up in the foam. This model assumes that the drag force per unit volume for each fluid is a function of the relative permeability, f_α, of each phase. Stemmet et al.[105] correlated the static hold-up as a function of the Eötvös number, for foams in the range 5 to 40 PPI, see Figure 29. They fitted their data with the model developed by Saez and Carbonell.[106] The total liquid hold-up data and fitted model results for 5 PPI foam are presented in Figure 30. The liquid holdup is not predicted well in the low liquid hold-up region, probably because it is highly dependent on the static hold-up. Stemmet et al.[100] also showed that the liquid holdup increases with increasing PPI, because the foam with a higher PPI has a higher specific surface area that gives a higher restriction to the flowing liquid.

A graph of mass transfer coefficient per liquid volume for 10 and 40 PPI solid foam for different liquid velocities in the co-current upflow configuration is given in Figure 31. Measurements were carried out by Stemmet et al.[101] in the pulsing regime where the interaction between gas and liquid is strong. Therefore, high rates of mass transfer are expected per liquid volume ($0.1-1.2\ s^{-1}$). These high rates correspond to the fact that equilibrium conditions are achieved, i.e., oxygen is almost completely desorbed from the liquid. This can lead to a large error in the calculation of mass transfer coefficient, and therefore one has to be careful while scrutinizing mass transfer data obtained using a physical technique.

Table 9. Correlations for Hydrodynamic and Transport Parameters for Knitted Wire Packings

reference	correlations	method	geometric properties	operating conditions	comments
Patil and Sharma[94]	flow transition-trickle flow to pulse flow $L_{trans}\Psi/\epsilon = 33.592(G_{trans}/\lambda\epsilon)^2 - 162.37(G_{trans}/\lambda\epsilon) + 200.65$ valid for $0.005 \le u_L \le 0.045$ m/s and $0.99 \le u_G \le 1.76$ m/s flow transition-pulse flow to slug flow $L_{trans}\Psi/\epsilon = -0.6838\|(G_{trans}/\lambda\epsilon)^2 - 28.813(G_{trans}/\lambda\epsilon) + 122.79$ valid for $0.005 \le u_L \le 0.045$ m/s and $1.9 \le u_G \le 2.9$ m/s $\Psi = (\sigma_w/\sigma_L)[(\mu_L/\mu_w)(\rho_w/\rho_L)^2]^{0.33}$ $\lambda = [(\rho_G/\rho_{air})(\rho_L/\rho_w)]^{0.5}$	visual inspection, air−water system	150 mm long, 25 mm diameter, bulk density = 440 kg/m^3	co-current downflow $u_L = 0.002-0.045$ m/s $u_G = 0.5-8$ m/s	limited to air/water systems
Patil and Sharma[94]	gas−liquid interfacial area $a_e = a u_G^{\beta_1} u_L^{\beta_2}$ $\alpha = 5970\ \beta_1 = 0.156\ \beta_2 = 0.514$ for trickle flow $\alpha = 1772\ \beta_1 = 0.267\ \beta_2 = 0.316$ for pulse flow $\alpha = 141660\ \beta_1 = 0.526\ \beta_2 = 1.33$ for slug flow	air oxidation of alkaline aqueous sodium dithionite solution	150 mm long, 25 mm diam, bulk density = 440 kg/m^3, 1.02 m long, 0.15 m i.d.	co-current downflow $u_L = 0.001-0.03$ m/s $u_G = 0.5-2.5$ m/s	also tested for low surface tension liquids, correlation developed for all regimes $a_e \propto u_G^{0.15}\, u_L^{0.5}$
Weiland et al.[76]	gas−liquid interfacial area in film flow $a_e = 356(u_G\rho_G^{1/2})^{-0.2}$	lean CO_2 absorption with chemical reaction in aqueous NaOH		countercurrent $u_L = 0.0028-0.011$ m/s $u_G = 0.46-1.0$ m/s	valid only for aqueous systems, dependence on gas velocity
Niranjan et al.[93]	gas−liquid interfacial area in film flow gas−liquid interfacial area remained constant over the entire range of gas and liquid velocities	lean CO_2 absorption with chemical reaction in aqueous NaOH	1.05 m long, 0.1 and 0.2 m column diameter	counter-current $u_L = 0.0005-0.0044$ m/s $u_G = 0.4-1.14$ m/s	valid only for aqueous systems, no dependence on gas and liquid velocity $a_e \sim$ constant
Niranjan et al.[93]	liquid hold-up in film flow $\beta_L = 0.784 u_L^{0.28}$	weighing technique, dynamic hold-up, air and water system	1.05 m long, 0.2 m column diameter	counter-current $u_L = 0.001-0.0075$ m/s $u_g = 0-0.3$ m/s	valid only for aqueous systems, β_L should depend on liquid film thickness, as a_e is constant
Patil and Sharma[94]	pressure drop $\frac{\left(\frac{dp}{dz}\right)_{irrigated}}{\left(\frac{dp}{dz}\right)_{dry}} = 1 + \beta_3 Re_G + \beta_4 Re_L$ $\beta_3 = 70.2 \times 10^5$ $\beta_4 = 67 \times 10^3$ for trickle flow $\beta_3 = -27.6 \times 10^5$ $\beta_4 = 72.3 \times 10^3$ for pulse flow $\beta_3 = 13.2 \times 10^5$ $\beta_4 = 34 \times 10^3$ for slug flow	manometer reading	150 mm long, 25 mm diameter, bulk density = 440 kg/m^3	co-current downflow $u_L = 0.002-0.045$ m/s $u_L = 0.5-8$ m/s	valid only for aqueous systems
Weiland et al.[76]	gas−liquid mass transfer in film flow $Sh_L = 3.4 Re_L^{-0.08} Sc_L^{1/2}$	lean CO_2 absorption with chemical reaction in aqueous $Na_2CO_3 + NaHCO_3$	1.02 m long, 0.15 m id	co-current $u_L = 0.0028-0.011$ m/s $u_G = 0.46-1.0$ m/s	valid only for aqueous systems, negative dependence on liquid velocity $k_L \propto u_L^{-0.08}$
Niranjan et al.[93]	gas−liquid mass transfer in film flow no correlation developed	lean CO_2 absorption with chemical reaction in aqueous $Na_2CO_3 + NaHCO_3$	1.05 m long, 0.2 m column diameter	counter-current $u_L = 0.001-0.0075$ m/s $u_G = 0-0.3$ m/s	valid only for aqueous systems $k_L \propto u_L^{0.2}$

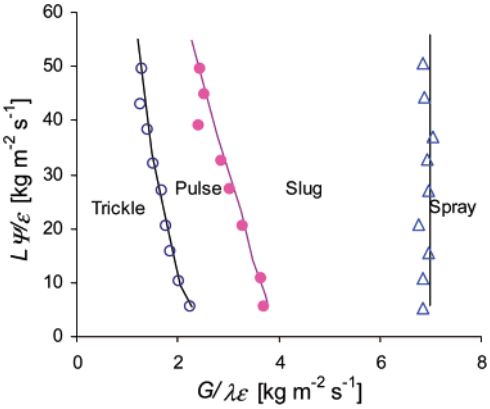

Figure 26. Flow map for knitted wire packing (air−water system).[94] $\Psi = \sigma_{water}/\sigma_L\ [\mu_L/\mu_{water}(\rho_{water}/\rho_L)^2]^{0.33}$; $\lambda = [\rho_G/\rho_{air}(\rho_L/\rho_{water})]^{0.5}$.

The axial dispersion coefficient values obtained by Stemmet et al.[101] were at least two orders of magnitude larger than those obtained by Montillet et al.,[97] who found that $D_{ax,L}$ increases with liquid superficial velocity (see Table 11 and Figure 32). This is not surprising since Stemmet et al.[101] performed RTD experiments with three time's higher liquid velocity. Stemmet et al.,[101] used the co-current up-flow mode which results in large axial mixing while Montillet et al.[97] worked in the down-flow mode. Stemmet et al.[101] concluded that axial dispersion ($B_o \geq 10$ at $u_L = 0.02-0.1$ m/s and $u_G = 0.1-1.0$ m/s) had negligible effect on the calculated mass transfer coefficients.

Richardson et al.[96] measured gas phase overall wall heat transfer coefficient, U in 30 PPI ceramic foams. They compared the results obtained for the ceramic foam with conventional 0.5 mm glass spheres with equivalent diameter, i.e., the same surface to volume ratio. Figure 33 shows a comparison between the Nusselt numbers at 800 °C for 30 PPI foam, measured experimentally, and for 0.5 mm glass spheres calculated from an analogous expression for spheres. The foam shows a higher Nusselt number by about a factor of 4, except for low Reynolds numbers. It is evident that the convective heat transport in foams is far superior to that in packed beds of spheres with only gas flowing through the foam.

The aluminum foam from ERGAerospace is used as a compact heat exchanger.[27] The ligament structure of Duocel aluminum foam promotes complete mixing and efficient scrubbing of the heat exchange surfaces. All aluminum brazed joints provide continuous, highly conductive heat paths and superior overall thermal conductivity, all at less than 10% the weight of solid aluminum.

A novel technique for fabricating high-thermal-conductivity pitch-based carbon foams has been developed and patented at the Oak Ridge National Laboratory.[107] They produce graphite foams with a thermal conductivity equivalent to aluminum alloys at one-fifth of their weight. It has an open porous structure with surface areas 100 times greater than conventional heat exchangers. The bulk thermal conductivity of the 25% dense graphite foam is 180 W/(m K) as compared to 15 W/(m K) of aluminum and 40 W/(m K) of copper foam. Applications for the ORNL graphite foam that are currently being explored are as follows: Power electronics cooling with 10 times larger cooling potential than traditional heat sinks and in radiators. Experiments have demonstrated that the overall heat transfer coefficient is very high compared to that of a standard automobile radiator (2500 W/(m^2 K) vs 30 W/(m^2 K)).

From the above it appears that the radial thermal conductivity through the foam structure can be high compared to randomly packed beds. It should be noted that nothing is reported on the wall heat transfer coefficient, as it can be the limiting factor for heat transfer for highly exothermic reactions carried out in small diameter tubes.

7. Discussion

From previous sections, it can be concluded that structured multiphase reactors has inspired many groups both form academia and industry to focus (part of) their research effort on this developing field. In many aspects, a wealth of results can be found in scientific and patent literature, but not surprisingly, still large gaps are clearly there. With respect to hydrodynamics, pressure drop, and mass transfer rates, sufficient phenomena related information and correlations have been published with respect to monoliths and corrugated open crossflow structures, but only limited knowledge is available for multifilament wire mesh, foams, and corrugated closed crossflow structures. Regarding liquid solid mass transfer for monoliths and OCFS packings some basic experimental work has been done. Axial mixing in monoliths, OCFS and foams and the RTD due to maldistribution are the underlying phenomena causing "axial dispersion", which is clearly documented.

Despite the fact that the there are still many unknown areas, it is possible to get for most applications a sufficiently complete picture from an evaluation of existing information on the structured packings based on a critical assessment of three aspects that the authors think are relevant, namely the following ones: (1) type of experiments conducted; (2) measurement techniques used; and (3) hydrodynamic models applied.

7.1. Types of Experiments. In general, there has been done a vast amount of work on aqueous systems as the measurement techniques are well-known for such systems and moreover aqueous systems are easy to handle. Except for some of the pressure drop and liquid hold-up studies, experiments have been carried out primarily with aqueous solutions. This limits the use of the correlations for other fluid systems, for, e.g., organic systems, which are mostly applied in industrial applications. Flow transitions shift to lower superficial gas and liquid velocities when a low surface tension liquid is used.[108] This

Table 10. k_La_e and a_e Values for Knitted Wire Packing from Different Authors

authors	range of gas and liquid velocities	k_La_e (s^{-1})	dependence of k_La_e on gas and liquid velocity	a_e (m^2/m^3)	dependence of a_e on gas and liquid velocity
Patil and Sharma[94]	co-current downflow $u_L = 0.002-0.045$ m/s $u_G = 0.5-8$ m/s	−	−	150−400	$a_e \propto u_G^{0.15}u_L^{0.5}$
Weiland et al.[76]	co-current downflow $u_L = 0.0028-0.011$ m/s $u_G = 0.46-1.0$	0.015−0.02	$k_L \propto u_L^{-0.08}$	350−450	$a_e \propto u_G^{-0.2}$
Niranjan et al.[93]	counter-current $u_L = 0.001-0.0075$ m/s $u_G = 0-0.3$ m/s	0.02−0.05	$k_L \propto \mu_L^{0.2}$	450−500	−

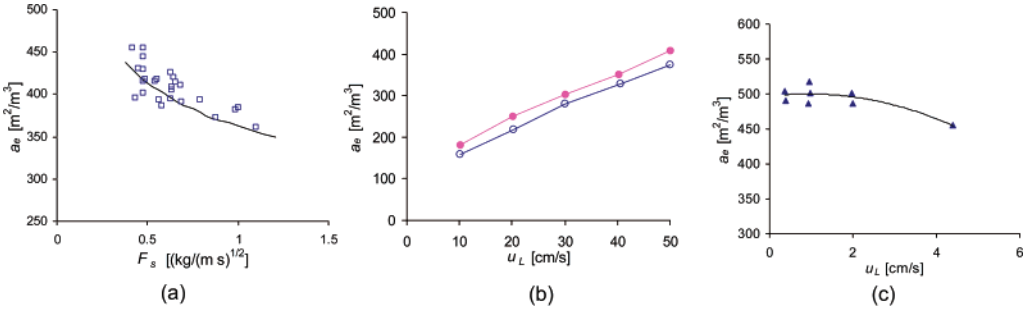

Figure 27. Comparison of the effective interfacial area, a_e (m^2/m^3) measured by three different authors: (a) Weiland et al.[76] on Goodloe packings, (b) Patil and Sharma[94] on HYFlux packings at (●) $u_G = 1$ m/s and (○) $u_G = 2$ m/s, and (c) Niranjan et al.[93] on HYFlux between $u_G = 0.4$ and 1.14 m/s.

can be explained from a decrease in surface tension causing an increase of liquid dynamic hold-up and thus, an increase of the probability for the flow channels to be blocked; see Figure 34. Further work is needed in this respect so that generalized correlations can be obtained to predict hydrodynamic parameters also for liquids with different surface tensions and viscosities.

Only limited experimental data has been reported on the heat transport characteristics from the packing to the heat transfer fluid for structured packings. This is quite understandable, since most of the discussed packings were used in distillation processes, and, as a consequence, there was no urge to determine the heat transfer capacity of these packings. In distillation processes, the main operation taking place is separation of fluids, in which there is no evolution or absorption of large amounts of heat unlike reactive processes. So, heat transfer is no issue. The first heat transfer studies carried out on these packings, e.g., metal monoliths and corrugated open crossflow structure were for gas-phase reactions. The results obtained show a lot of promise, e.g., very good heat transfer performance of metal monoliths. Therefore, it is indeed a right moment to put effort on the research of heat transfer characteristics of structured packings for multiphase applications.

7.2. Measurement Techniques. In order to get a good appreciation of the correlations presented in literature, it is crucial to discuss the techniques used to measure gas to liquid mass transfer rates in the packing. Several authors have reported k_La_e values, which were determined using physical methods and represent the gas−liquid mass transfer rates without chemical reaction. In the case of a physical method, which involves the transfer of a sparingly soluble gas into liquid, care has to be taken that the saturation value of the gas in the liquid is not approached, leading to inaccuracies in the determination of k_La_e. This poses a serious limitation for the structured packings where mass transfer rates are often very high. The high geometric surface areas of many structured packings makes it even more difficult to carry out reliable experiments as the saturation value is reached after a relatively short length. Therefore, short lengths are used and end effects cannot be neglected. So, it is obvious that compared to classical packings measurements with structured packings deserve more care because of their often high mass transfer rates.

7.3. Hydrodynamic Models. There is ample information available regarding hydrodynamic models applicable to monoliths and open crossflow structures. Many authors summarized their data in the form of correlations. However, they are usually valid only within a certain regime of operation and at the same time they often have not been validated for low surface tension and high viscosity liquids. We strongly recommend the use of physical phenomena or mechanism related models as compared to (semi-)empirical correlations as they are much more realistic and can be applied in general to any packing. A good example to show this is the phenomenological model for pressure drop in film flow monoliths based on a channel model developed by Lebens et al.[54] that can be applied to any packing. Similarly, the pressure drop model developed by Stichlmair et al.[38] based on a particle model can also be used for a packed bed reactor. Since these models are based on physical phenomena occurring in the channels, the principles on which the model is based can be applied both to co-current and counter-current mode, provided the hydrodynamic picture is similar. It is remarkable that RTD measurements show large differences, even for monolithic reactors, that are relatively well-defined. In many, if not all, cases where broad RTDs are reported this is due to maldistributions occurring easily in structured reactors because of the inherent low friction.[65]

Unfortunately, models based on a full-fledged validation of experimental data are rarely found. A rare example of such validation is the work of Lebens et al.[48] with respect to liquid hold-up in film flow monoliths. He developed a correlation for liquid hold-up with experimental data validated for liquids of different viscosities, surface tensions and geometries. It is important to appreciate the flexibility of such a correlation as compared to the one, which is not validated over various relevant variables.

8. Industrial Applications of Structured Packings

We expect that the research on the application of structured packings for reactions with strong diffusional limitations, pressure drop constraints and heat transfer limitations will be intensified in the next years due to their obvious benefits over random beds. To sum up, we outline a few applications how the geometry of the structured packing giving rise to useful hydrodynamic properties can be exploited to the maximum. A main industrial application of structured packings will be for a multitubular fixed bed reactor in which the tubes are packed with structured catalysts instead of the conventional catalyst particles. Another unique application of structures such as ceramic monoliths is an adiabatic loop reactor where the heat is removed in an external heat exchanger. Such a configuration is an easy way to replace a slurry reactor.

8.1. Structured Multitubular Fixed Bed Reactor. This concept can be an ideal retrofit for processes operated in multiples of small diameter tubes packed with catalyst. An excellent example for this application would be the Fischer−Tropsch (F−T) synthesis, which is an exothermic reaction carried out in multitube reactors.[70] This application suffers mainly from pressure drop limitations, the difficulty to remove the heat of reaction, and ineffective catalyst utilization. Since the rate of reaction is the highest near the entrance, the possibility of developing a hot-spot near the entrance that might lead to a decrease in selectivity or even a runaway is high. A

Table 11. Correlations for Hydrodynamic and Transport Parameters for Foams

reference	correlations	method	geometric properties	operating conditions	comments
Richardson et al.[102]	dry pressure drop $dp/dz = a_0 u_G + a_1 u_G{}^2$ $a_0 = A a_g{}^2 \mu(1-\epsilon)^2/\epsilon^3$, $a_1 = B a_g \rho(1-\epsilon)/\epsilon^3$ $A = 9.73 \times 10^2 d_p{}^{0.743}(1-\epsilon)^{-0.0982}$ $B = 3.68 \times 10^2 d_p{}^{-0.7523}(1-\epsilon)^{0.07158}$	dry pressure drop measured with differential pressure transducer	10−65 PPI of α-alumina foams	$u_G = 1-7$ m/s	experimental dry pressure, drop data follow the Forchheimer equation, parameters A and B depend on the media properties
Stemmet et al.[105]	static liquid holdup $S_L^0 = \epsilon_L^0/\epsilon = [\epsilon(9 + 0.025Eo^*)]^{-1}$ total liquid holdup (relative permeability model of Saez and Carbonell[106]) $F_\alpha/\epsilon_\alpha = 1/f_\alpha(S_\alpha)(ARe_\alpha/Ga_\alpha + BRe_\alpha{}^2/Ga_\alpha)\rho_\alpha g$ $\alpha = G,L$ $S_\alpha = \epsilon_\alpha/\epsilon$, $f_G = S_G^{n_1}$, $f_L = (S_L - S_L^0/1 - S_L^0)^{n_2}$ 5 PPI: $A = 8.31 \times 10^5$, $B = 25.09$, $n_1 = 5.17$, $n_2 = 2.33$ 20 PPI: $A = 42.1 \times 10^5$, $B = 14.03$, $n_1 = 3.88$, $n_2 = 1.55$ 40 PPI: $A = 0.088 \times 10^5$, $B = 5.04$, $n_1 = 4.25$, $n_2 = 1.73$	measuring the liquid holdup, by a weighing technique	5−40 PPI Al foam, 30 cm × 1 cm × 80 cm height, $\epsilon = 0.92 - 0.94$	counter-current $u_L = 0-0.03$ m/s $u_G = 0-0.8$ m/s	relative permeability model adequately describes the liquid holdup in the high liquid hold-up regime in foams
Stemmet et al.[101]	gas−liquid mass transfer no correlation available	physical desorption of oxygen from water with nitrogen	10 and 40 PPI Al foam, 30 cm × 1 cm × 30/60/90 cm height, $\epsilon = 0.92 - 0.94$	co-current upflow $u_L = 0-0.1$ m/s $u_G = 0-0.8$ m/s	prediction of $k_L a_e$ values per liquid vol between $0.05-0.6$ s^{-1}
Montillet et al.[97]	residence time distribution of liquid $D_{ax} = 1.26 \times 10^{-3} u_L$ for 45 PPI foam $D_{ax} = 1.01 \times 10^{-3} u_L$ for 60 PPI foam	dynamic tracer technique using polarographic method	45 and 60 PPI Ni foam	liquid phase only $u_L = 1.1 \times 10^{-3} - 8.9 \times 10^{-3}$ m/s	aqueous system used, no effect of gas flow studied, axial dispersion found to be limited
Stemmet et al.[101]	residence time distribution of liquid $Bo_L = u_L Z/(D_{ax,L}\epsilon_L) = 19$ at $u_L = 0.02$ m/s and $u_G = 0.1$ m/s $Bo_L = u_L Z/(D_{ax,L}\epsilon_L) = 50$ at $u_L = 0.02$ m/s and $u_G = 1.0$ m/s	dynamic tracer technique by measuring conductivity nitrogen/water system, with KCl as tracer	10 PPI aluminum foam, 30 cm × 1 cm × 30/60/90 cm height, $\epsilon = 0.92 - 0.94$	co-current up flow $u_L = 0.02-0.1$ m/s $u_G = 0.1-1.0$ m/s	$D_{ax,L} \propto 1/u_G$
Richardson et al.[96]	overall heat transfer coefficient $Ud_t/\lambda_f = 2.49 \times 10^{-8} \epsilon T^3 + 12.6 Re_s$	measuring outlet temperature for different air flow rates	30 PPI ceramic foams, $\epsilon = 0.82$, $a_g = 26200$ m^2/m^3, $a_P = 4720$ m^2/m^3	inlet $T = 650-850$ °C, air flow rates up to 50 m^3/min	radiation effects included in the correlation

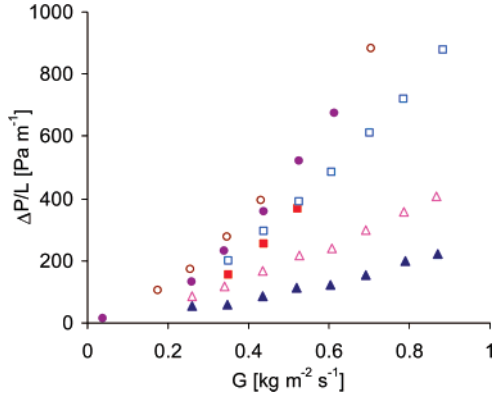

Figure 28. Pressure drop per unit length for 5 PPI and 40 PPI aluminum foam in the trickle flow regime.[100] 5 PPI: (▲) only gas; (■) L = 10.3 kg/(m^2 s); (●) L = 17.2 kg/(m^2 s). 40 ppi: (△) only gas; (□) L = 10.3 kg/(m^2 s); (○) L = 17.2 kg/(m^2 s).

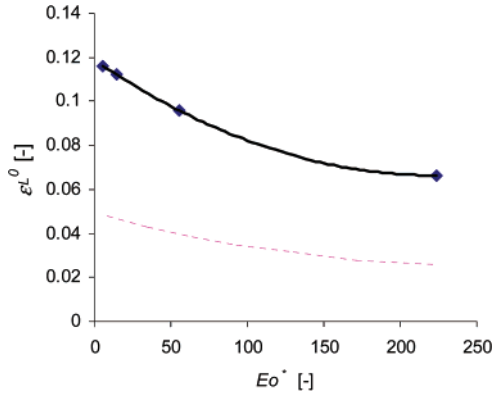

Figure 29. Static liquid holdup, $\epsilon_L{}^0$ for aluminum foam packings in the range 5 to 40 PPI, plotted against the Eötvös number, *Eo**: (--) model of Saez and Carbonell;[106] and (◆) model of Stemmet et al.[105]

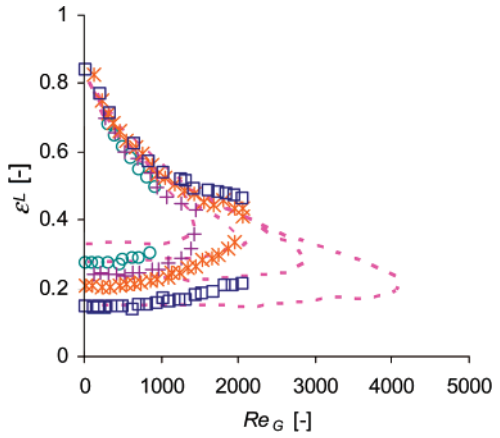

Figure 30. Data and modeling results of the liquid holdup versus Re_G using model of Saez and Carbonell[106] for a 5 PPI aluminum foam.[105] Low liquid hold-up (trickle flow): bottom increasing trend, high liquid hold-up (bubble and pulsing flow): top decreasing trend, (□) Re_L = 295; (∗) Re_L = 593; (+) Re_L = 889; (○) Re_L = 1185; (···) model.

profiled catalytic activity along the reactor bed in which the catalyst loading is varied can effectively help in reducing the hot spots at the entrance. If a catalyst coating is applied on a structured backbone, the loading can be varied within limits by changing the coating thickness. The coating thickness would have no effect on the hydrodynamics, as the hydrodynamics will be determined entirely by the geometry of the structure.

Another interesting alternative to the option of decreasing productivity at the entrance is to improve the radial heat transport without a proportional increase in pressure drop. The radial heat

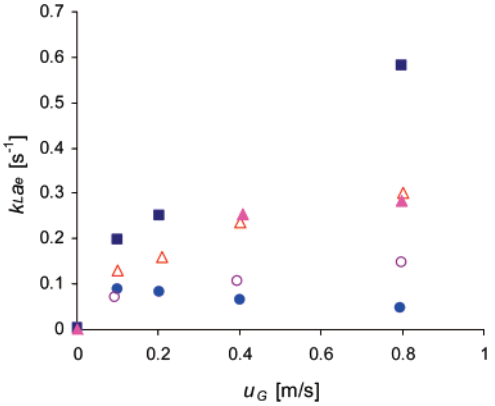

Figure 31. Mass transfer coefficient per reactor volume for 10 and 40 (PPI) aluminum foam packings for different liquid velocities in the co-current upflow configuration: (●) 10 PPI, u_L = 0.02 m/s; (○) 40 PPI, u_L = 0.02 m/s; (▲) u_L = 0.04 m/s; and (■) 10 PPI, u_L = 0.1 m/s.[101]

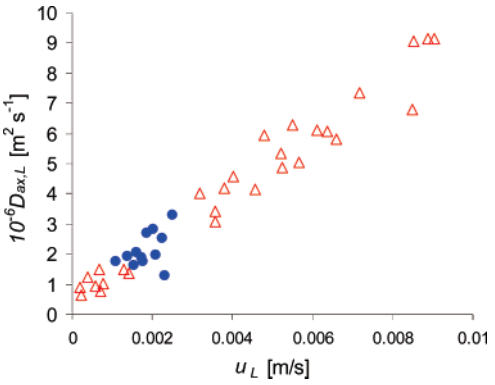

Figure 32. Axial dispersion coefficient versus superficial liquid velocity for (●) 45 PPI nickel foam and (△) 60 PPI nickel foam.[101]

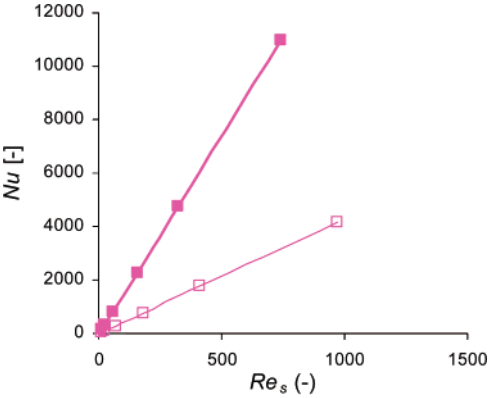

Figure 33. *Nu* as a function of Re_s for (■) 30 PPI ceramic foam and (□) 0.5 mm glass spheres at 800 °C.[96]

transport can be improved mainly in two ways. One option would be to intensify the conduction to improve the effective radial thermal conductivity and the other option would be to introduce radial convection, which is not based on mixing flow patterns. The concept of good radial conduction can be fulfilled by a combination of good heat conduction of the packing and maximizing the heat transfer at the wall. The former can be realized by applying a metal monolith with thicker walls, e.g., aluminum, copper, SiC etc. The latter benefits from a conducting contact with the wall (see section 6.1). Alternatively, radial convection at the wall can be introduced by applying a corrugated open or closed crossflow packing (see sections 6.2 and 6.3).

A third option can be to scale down the radial heat transport properties of the structured packing to enable low-pressure drop

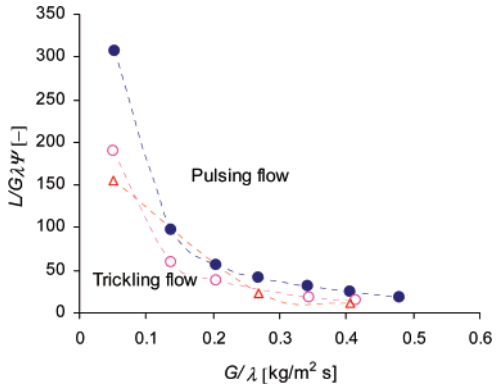

Figure 34. Flow pattern diagram, three-lobed extrudates: (●) air−water, (○) air−water + cmc; (△) air−water + $C_{12}H_{25}SO_3Na$.[108] λ and ψ have the same meaning as given in Figure 26.

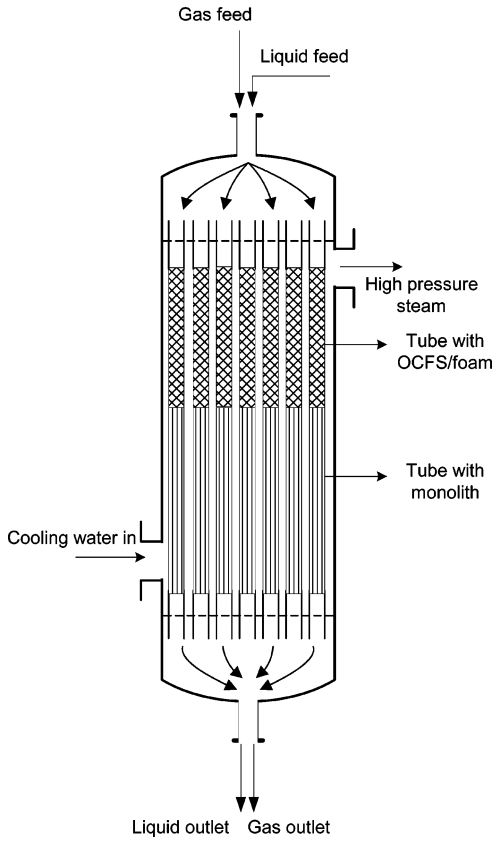

Figure 35. Schematic diagram of a multitubular fixed bed reactor with a crossflow structure in the first section of each tube followed by a monolith structure in the second section of each tube.

in regions where not much heat needs to be removed, i.e., in regions of low reactant concentration. An example for this option would be to choose for a corrugated closed crossflow structure or a metal monolith with a conducting contact with the wall for the first part of the reactor tube which demands substantial heat transfer rates followed by a monolith for the bottom part of the reactor tube, thus gaining on pressure-drop (Figure 35).

To summarize, the discussed structured packings can be considered for various applications having heat removal and/or pressure drop limitations. However, they should be optimized with respect to geometric and total surface area (which will be proportional to the catalyst hold-up), G-L/L-S mass transfer and pressure drop.

8.2. Adiabatic Loop Reactor. This concept can be applied when low conversion per pass is acceptable (Figure 36). This reactor concept very effectively decouples the heat and mass

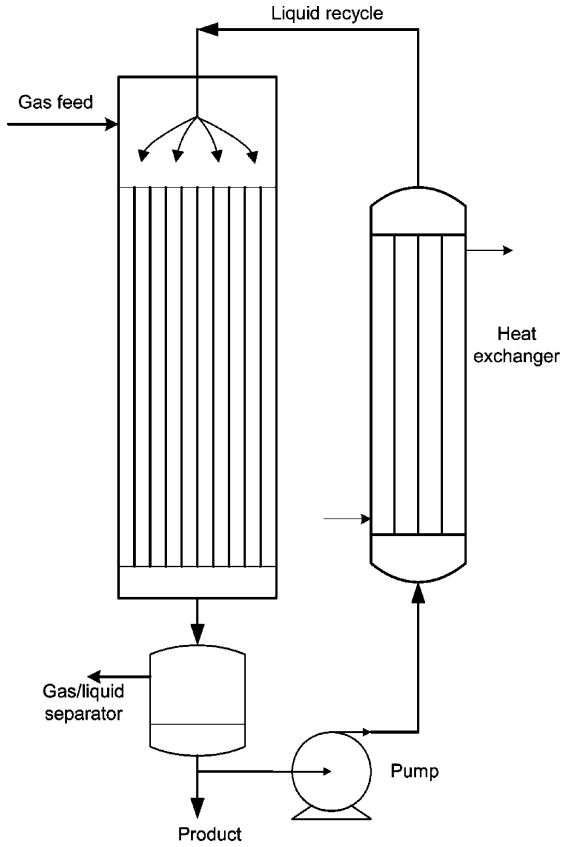

Figure 36. Schematic diagram of a monolith loop reactor with external heat exchanger.

transfer zones. The mass transfer takes place in the structured packing and the heat transfer takes place in the external heat exchanger where the heat of reaction is removed. The conversion per pass is kept limited to avoid unacceptable temperature rise in the reactor. An excellent example of a structured packing which can be used in such an application is a cordierite monolith. Because of its low thermal conductivity, it works as an adiabatic reactor. The combination of Taylor flow resulting in high mass transfer rates coupled with low-pressure drop at high liquid recirculation rates would result in a reactor configuration ideal for low conversions. In processes where higher conversion per pass is desired, an option would be to introduce staged energy removal. In this option, near-isothermal conditions can be achieved by removing the heat of reaction stage wise via liquid circulation through an external heat exchanger.

9. Comparison between Various Packings

A comparison between the various structured packings and a randomly packed bed is carried out in Table 12. The most important criteria, which are used to compare the various packings are as follows:

9.1. Catalyst Holdup. Structured packings typically have a catalyst holdup between 10 and 30%. At first sight this seems to be a major limitation for processes requiring high catalyst hold-up. On the other hand, new techniques are being developed in which with a good design the structured reactor can sustain high catalyst loads. A modeling study was carried out by Desmet et al.[109] to determine the optimal layer thickness in order to maximize productivity. It is even possible to produce structured reactors from catalyst material enabling essentially unlimited catalyst loading. Of course, this requires a large catalyst development program.

Table 12. Qualitative Comparison of Different Catalytic Packings in Multiphase Flow[a]

	packed bed (base case)	metal/ceramic monolith	OCFS	CCFS	knitted wire packing	metal foam
catalyst holdup	++	+	+	+	−[b]	+
short diffusion lengths	--	++	++	++	++	++
catalyst coating	N/A (++)	++	++	+	?	+
radial mixing for mass	±	--	++	+[c]	+	+
$k_L a_e/\Delta P$	-	++	++	++	++	+
axial dispersion	+	±[d]	++	++	?	+[e]
liquid to solid mass transfer	+	+	±	±	?	?
heat transport by convection	±	--	++	++	+	+
heat transport by conduction	--	+±	+	+	±	++
pressure drop	--	++	+	+	+	±
convenience for loading into the reactor tubes	±	±	±	±	++[f]	±

[a] Key: (++) high/very positive; (+) sufficient/positive; (±) moderate; (−) negative; (?) not available; (N/A) not applicable. These ratings should be regarded as a qualitative guideline to select the optimal packing. [b] The surface area provided by the multifilaments may be reduced after coating. [c] Because of the closed channels, the radial mixing can be lower than, e.g., OCFS. [d] Taylor flow in each channel is close to plug flow but the maldistribution effects over the complete monolith results into a significant axial dispersion. [e] Since foam can be considered as an inverted form of a random packed bed with a high porosity the axial dispersion effects can be similar. [f] Knitted wire packing is flexible and hence can be pushed along the reactor length easily. But it is not known if the coating will be sufficiently strong and stable to withstand the friction against the wall during the loading procedure.

9.2. Short Diffusion Lengths. In the case of fast reactions, pore diffusion limitation will occur already with particles of less than 1 mm. This is a realistic argument as due to the rapid development in the area of catalysis, highly active catalysts have been employed for several industrially relevant processes. In fact it is to be expected that "to be developed" novel generations of catalysts will be more active than the present ones. Thus, a catalyst coated structured reactor with the coating providing short diffusion lengths is the best alternative to a pore diffusion limited fixed bed reactor.

9.3. Catalyst Coating. It is important that the support matrix of the structure is able to retain the active catalytic material under severe conditions such as high flow rates, pressures, and temperatures. For most, but not all, packings, proven technologies for coating them with active material are available. Nevertheless, in developing a new process catalyst optimization might be a barrier also for "simple" structured packings.

9.4. Radial Mixing. Radial mixing is a strong function of geometric properties of the packing. If the geometry of the packing is such that it can create convection in the radial direction of the flow or turbulence, then the radial mixing properties of the packing are generally good. Efficient radial mixing leads to flat concentration and temperature profiles in the radial direction. The radial mixing characteristics are relevant in heat transport when radial convection plays an important role in determining the radial heat transport properties of a packing.

9.5. Gas to Liquid Mass Transfer. In multiphase reactor systems, where gas and liquid compounds react in the presence of a solid catalyst, or when the reactants are gases which have to dissolve in the liquid in order to reach the catalytic sites, the mass transfer rate between gas and liquid is important for efficient design of the reactor. Since gas to liquid mass transfer mainly depends upon the fluid properties and flow rates, it is possible to increase this rate but most of the times at the expense of pressure drop. The mass transfer rates obtained in random packings are comparable to those obtained in structured packings provided that the regime of operation is the same (low interaction) but at a much higher pressure drop. Moreover when it is possible to achieve Taylor flow conditions in the structured packings, then the mass transfer rates achieved are very high (see Figure 11) as compared to the random packings. Therefore, overall this makes the random packings highly inefficient in terms of the ratio of the mass transfer rate to the pressure drop: $k_L a_e/\Delta P$.

9.6. Axial Dispersion. In multiphase reactions, axial mixing of both gas and liquid phase is relevant in the case of positive order reactions because since both phases usually take part in the reaction, axial dispersion can decrease the effective concentrations along the length which would in turn affect the reaction rates. Thus, to minimize the adverse effects of axial mixing, better packing designs should be considered. For example, a high porosity packing with regular flow channels such as monolith or OCFS packing may reduce mixing in the gas phase. Similarly packings having good wetting characteristics may promote low levels of axial mixing in the liquid phase.[89] To support this, in processes where the packing material does not wet the process liquid, surface roughening or texturing can improve wetting properties of the material.[110] For monoliths Taylor flow in each channel is close to plug flow, but due to maldistribution over the channels, this may manifest itself as axial dispersion.[65]

9.7. Liquid to Solid Mass Transfer. L-S mass transfer mainly depends on the wetted area and the degree of turbulence in the liquid phase. Stagnant liquid around the catalyst is not desired because it decreases the intrinsic liquid−solid mass transfer coefficient, k_{LS}. As said earlier, packings with good wetting characteristics will help increasing the wetted area. Moreover surfaces which promote turbulence in the liquid-phase, resulting in not only liquid films but also drops, jets, and sprays, help to increase the interaction between the liquid and the solid surface. Monoliths operated in Taylor flow are not as efficient in transferring the liquid to the solid surface as they are in transferring the gas to the liquid phase. This is due to the presence of a liquid film on the channel walls which limits the mass transfer process as the mass is transferred through this film only by diffusion. It is important to maximize the geometric surface area and to reduce the thickness of the liquid film, by selecting the optimal conditions.

Heat transport in the radial direction is a result of two effects: conduction of the packing and fluids and convection. Depending on the packing geometry and packing material, either of the two effects is relevant for a particular case.

9.8. Heat Transport by Convection. Convective heat transport from the packing to the wall of the reactor tube is the primary mechanism in packings where convection of mass is predominant. Good heat transport in the radial direction is a result of efficient radial mixing properties of the packing.

9.9. Heat Transport by Conduction. In certain packings such as the monoliths, convective heat transport is completely absent. Nevertheless, the thermally connected nature of such packings provides in principle for an alternative mechanism of radial heat transport namely conductive heat transport. If suitable

materials, such as copper, aluminum, etc., and geometries are adopted then the thermal conduction through the solid phase can become significant.

Apart from these most important criteria, there are other factors that are also relevant for the comparison, i.e., pressure drop and easiness of loading. All the structured packings are characterized by a relatively low-pressure drop. Loading of the structured packings can be as cumbersome as particles. Because of the defined gap between the structure and the reactor wall, packing methods can be used for, e.g., monoliths, which will improve the heat transfer near the wall but at the same time will put their practical feasibility and ease of loading into question. Table 12 summarizes the most important properties of structured packings and rates them in comparison to a randomly packed bed reactor. The rating is largely based on a combination of results obtained for single-phase flow and ongoing research in our group on determination of heat and mass transfer rates in the mentioned structured packings.

10. Outlook

Changing from a random packing to a structured packing would mean aiming for process-intensification as the new reactor-type will result in a higher productivity per cubic meter of reactor volume and higher selectivity compared to the traditional randomly packed bed reactor. Structures with high radial conductivity will enable going to larger tube diameters in fixed bed operation. This will not only reduce the material costs but also ease out the loading and unloading procedures as fewer tubes will be required.

Substantial amount of research still needs to be done on determining and possible improving of the heat transfer rates in the structured packings. If future work confirms the forecasted advantages of the structured packings over random packings, it will be a big boost for commercial processes in which the reactors suffer from heat transfer removal problems.

11. Conclusions

Structured packings are a promising alternative to the existing packed bed and slurry reactors. They show flexibility with respect to catalyst holdup, hydrodynamic regimes attainable, pressure drop, flow rates, and heat transfer properties, which is not often seen in packed bed reactors. They are important for Process Intensification. It is striking that unprecedented high mass transfer rates can be achieved on the one hand by intense turbulence and on the other hand under laminar conditions. Compared with slurry reactors they are much more convenient and compact. With the fast progress in the area of catalysis, it is not too far from now that structured packings will overcome the disadvantage of lower catalyst holdups and higher costs over their obvious advantages of higher reaction rates and selectivities, lower pressure drop, and better heat removal when compared to packed bed reactors. Unlike packed bed reactors, structured packings allow the decoupling of intrinsic kinetics, transport phenomena, and hydrodynamics making them far more flexible in all respects.

Still, more work needs to be carried out to quantify the heat transfer rates in two-phase flow. Since the heat transfer rates in single phase flow operation show a lot of promise, it is worthwhile to spend effort on investigating the heat transport phenomena in two-phase flow systems. After analyzing the gas phase heat transport studies, we believe that heat transfer characteristics of the packings will have an edge over that of randomly packed beds in two-phase flow due to the much effective radial transport of mass generated from the turbulence created by gas−liquid flow which leads to a better transport of heat as well. There are several correlations available on phenomena based pressure drop models, which theoretically can be applied to any packing provided the prevalent hydrodynamics support the underlying phenomena. Moreover existing correlations, though mostly developed for aqueous (water−air) systems, already give us sufficient information to look for when we want to extend them to other systems. Of course, ultimately the validation of these models with experimental data is necessary to substantiate their application in co-current two-phase flow applications. Particularly experimental studies with lower surface tension liquids deserve attention as surface tension has a strong effect on the contact angle and wetting characteristics affecting mainly interfacial area and liquid holdup.

Last, but not least, residence time distributions in structured reactors must be well considered, maldistributions in the gas−liquid flow may turn their advantage into a disadvantage, although for monoliths the influence on the conversion is limited.[66]

Nomenclature

a_e = gas−liquid interfacial area ($m^2/m_{reactor/liquid}^3$)
a_g = geometric surface area per unit volume of solid (m^2/m_{solid}^3)
a_{LS} = liquid−solid interfacial area (m^2/m_{solid}^3)
a_p = geometric surface area ($m^2/m_{reactor}^3$)
B = channel base (mm)
Bo_L = liquid Bodenstein number; $Bo_L = u_L Z/(D_{ax,L}\epsilon_L)$
Ca = Carberry number, $\eta u/\sigma$
CPSI = no. of cells per square inch (cells/in.^{2})
d_b = bubble diameter (m)
d_c = channel diameter (m)
d_{cap} = capillary diameter (m)
d_e = equivalent diameter (m)
d_h = hydraulic diameter (m)
d_m = average strand diameter (mm)
d_p = pore diameter (mm)
d_t = tube diameter (m)
$D_{ax,L}$ = liquid phase axial diffusion coefficient (m^2/s)
D_L = liquid diffusivity (m^2/s)
Eo^* = modified Eötvos number; $Eo^* = \rho_L g d_e^2 \epsilon/[\sigma(1-\epsilon)^2]$
F = interfacial force (kg/(m/s))
f = relative permeability
Fr = Froude number; $Fr = u/\sqrt{g d_h}$
G = gas mass velocity (kg/(m^2 s))
G_{trans} = gas mass velocity at transition (kg/(m^2 s))
Ga = Galileo number; $Ga = g d_h^3 \rho^2/\mu^2$
Gz = Graetz number; $Gz = Re_L Sc_L \delta/H$
h = crimp height of packing (mm)
H = flow distance (m)
Ka = Kapitsa number; $Ka = \sigma_L^3 \rho_L/(\mu_L^4 g)$
k_L = liquid side intrinsic mass transfer coefficient (m/s)
k_{LS} = liquid−solid intrinsic mass transfer coefficient (m/s)
$k_L a_e$ = gas to liquid mass transfer coefficient (s^{-1})
k_w = thermal conductivity of washcoat (W/(m K))
k_s = thermal conductivity of support
K = parameter, which is a function of packing (W/(m K))
l = capillary length (m)
L = liquid mass velocity (kg/(m^2 s))
L_{bubble} = bubble length (m)
L_{slug} = slug length (m)
L_{trans} = liquid mass velocity at transition (kg/(m^2 s))
N = no. of pores per inch (PPI) of the foam (in.$^{-1}$)
Nu = Nusselt number; $Nu = U d_t/\lambda_f$
PPI = pores per inch foam pore density
Pe_f = Peclet number based on channel size; $Pe_f = u_L d_c/(D_{ax,L})$

$(-dp/dz)_{irrigated}$ = irrigated pressure drop (with liquid) (Pa/m)
$(-dp/dz)_{dry}$ = dry pressure drop (Pa/m)
Q_L = liquid flow rate (L/h or $m^3/(m^2\ h)$)
Q_G = gas flow rate (L/h or $m^3/(m^2\ h)$)
Re_G = Reynolds number based on superficial gas velocity
$Re_{G,eff}$ = Reynolds number based on effective gas velocity; $Re_{G,eff} = \rho u_{G,eff} d_h/\mu_G$
Re_L = Reynolds number based on superficial liquid velocity; $Re_L = \rho u_L d_h/\mu_L$
Re_s = Reynolds number based on external surface area per volume of solid, $\rho u_L/a_g\mu_L$
S = channel side of packing
$S_L^0 = \epsilon_L^0/\epsilon$ = saturation of liquid at static hold-up condition
$S_L = \epsilon_L/\epsilon$ = saturation of liquid at total hold-up condition
Sc = Schmidt number; $Sc = \mu_L/\rho_L D_L$
Sh_L = Sherwood number for gas−liquid mass transfer; $Sh_L = k_L 4\delta/D_L$, $k_L d_b/D_L$
Sh_{LS} = Sherwood number for liquid−solid mass transfer
Sh_{ave} = average Sherwood number; $Sh_{ave} = k_L\delta/D_L$
T = temperature (K)
U = overall wall heat transfer coefficient ($W/(m^2\ s\ K)$)
$u_{ave,film}$ = average total velocity in liquid film (m/s)
u_G = superficial gas velocity (m/s)
$u_{G,eff}$ = effective gas velocity (m/s)
$u_{G,trans}$ = gas velocity at flow transition (m/s)
u_L = superficial liquid velocity (m/s)
$u_{L,eff}$ = interstitial liquid velocity (m/s)
$u_{L,trans}$ = superficial liquid velocity at flow transition (m/s)
u_{TP} = unit cell velocity ($u_L + u_G$) (m/s)
We = Weber number, $u\rho d_h/(\sigma g)$
y_m = mixed cup concentration of gas in the liquid film
Z = column height (m)

Greek Letters

α = slope of the steepest descent line with respect to the horizontal axis (deg)
α_w = wall heat transfer coefficient ($W/(m^2\ K)$)
$\beta_{G,Taylor}$ = ratio of gas slug length to total slug length
β_L = liquid hold-up based on void volume
β_{W0} = static liquid hold-up for water
χ = tortuosity of the strands
δ = liquid film thickness (m)
ϵ = void fraction
ϵ_s = solid fraction
ϵ_L = liquid hold-up
ϕ^2 = dimensionless pressure gradient ratio
γ = contact angle (deg)
$\lambda_{e,r}$ = radial effective thermal conductivity (W/(m K))
λ_f = thermal conductivity of the fluid (W/(m K))
λ_s = thermal conductivity of the metal monolith (W/(m K))
λ_w = thermal conductivity of the washcoat (W/(m K))
μ_G = dynamic viscosity of gas (cP)
μ_L = dynamic viscosity of liquid (cP)
μ_W = dynamic viscosity of water (cP)
ζ = dimensionless length
ξ = washcoat fraction
ρ = fluid density (kg/m^3)
ψ_L = dimensionless slug length; $\psi_L = L_{slug}/d_c$
T = linear liquid flow, based on perimeter (kg/(m s))
θ = angle with horizontal for corrugation channel (deg)

Literature Cited

(1) Dudukovic, M. P.; Larachi, F.; Mills, P. L. Multiphase reactors−revisited. *Chem. Eng. Sci.* **1999**, *54*, 1975−1995.

(2) Dudukovic, M. P.; Larachi, F.; Mills, P. L. Multiphase catalytic reactors: a perspective on current knowledge and future trends. *Catal. Rev.* **2002**, *44* (1), 123−246.

(3) Al-Dahhan, M. H.; Larachi, F.; Dudukovic, M. P.; Laurent, A. High Pressure Trickle-Bed Reactors−A Review. *Ind. Eng. Chem. Res.* **1997**, *36*, 3292−3314.

(4) Kapteijn, F.; Heiszwolf, J. J.; Nijhuis, T. A.; Moulijn, J. A. Monoliths in multiphase catalytic processes−aspects and prospects. *Cattech* **1999**, *3* (1), 23−40.

(5) Kapteijn, F.; Nijhuis, T. A.; Heiszwolf, J. J.; Moulijn, J. A. New non-traditional multiphase catalytic reactors based on monolithic structures. *Catal. Today* **2001**, *66*, 133−144.

(6) Cybulski, A.; Moulijn, J. A. Monoliths in heterogeneous catalysis. *Catal. Rev. Sci. Eng.* **1994**, *36*, 179−270.

(7) Kreutzer, M. T.; Kapteijn, F.; Moulijn, J. A. Shouldn't catalysts shape up? Structured reactors in general and gas−liquid monolith reactors in particular. *Catal. Today* **2006**, *111*, 111−118.

(8) Moulijn, J. A.; Kreutzer, M. T.; Kapteijn, F. A little structure works wonders. *TCE* **2005**, 32−34.

(9) Spiegel, L.; Meier, W. Distillation columns with structured packings in the next decade. *Trans. Inst. Chem. Eng.* **2003**, *81*, 39−47.

(10) Laso, M.; de Brito, M. H.; Bomio, P.; von Stockar, U. Liquid-side Mass Transfer Characteristics of a Structured Packing. *Chem. Eng. J.* **1995**, *58*, 251−258.

(11) Frank, M. J. W.; Kuipers, J. A. M.; Versteeg, G. F.; van Swaaij, W. P. M. The Performance of Structured Packings in Trickle-Bed Reactors. *Trans. Inst. Chem. Eng.* **1999**, *77*, 567−582.

(12) Von Scala, C.; Moritz, P.; Michl, H.; Ramgraber, F. Process and device for hydrolytically obtaining a carboxylic acid and alcohol from the corresponding carboxylate. European Patent 1220825, January 12, 2003.

(13) Cybulski, A.; Moulijn, J. A. In *Structured Catalysts and Reactors*, 2nd Edition; Cybulski, A., Moulijn, J. A., Eds.; CRC Press, Boca Raton, FL, 2006; pp 1−16.

(14) Tronconi, E.; Groppi, G.; Boger, T.; Heibel, A. K. Monolithic Catalysts with High Conductivity, Honeycomb Supports for Gas/Solid Exothermic Reactions: Characterization of the Heat-Transfer Properties. *Chem. Eng. Sci.* **2004**, *59*, 4941−4949.

(15) DeLuca, J. P.; Campbell, L. E. Monolithic Catalyst Supports. In *Advanced Materials in Catalysis*; Burton, J. J., Garten, K. L., Eds.; Academic Press: London, 1977; pp 293−324.

(16) Pfefferle, L. D.; Pfefferle, W. C. Catalysis in Combustion. *Catal. Rev. Sci. Eng.* **1987**, *29*, 219−267.

(17) Konig, A.; Herding, G.; Hupfeld, B.; Richter, Th.; Weidmann, K. Current tasks and challenges for exhaust aftertreatment research−A viewpoint from the automotive industry. *Top. Catal.* **2001**, *16*, 23−31.

(18) Irandoust, S.; Andersson, B. Monolithic catalysts for nonautomobile applications. *Catal. Rev. Sci. Eng.* **1988**, *30*, 341−392.

(19) Banhart, J. Manufacture, characterisation and application of cellular metals and metal foams. *Prog. Mater. Sci.* **2001**, *46*, 559−632.

(20) Gallego, N. C.; Klett, J. W. Carbon foams for thermal management. *Carbon* **2003**, *41*, 1461−1466.

(21) Wen, X.; Afacan, A.; Nandakumar, K.; Chuang, K. T. Development of a novel vertical-sheet structured packing. *Chem. Eng. Res. Des.* **2005**, *83* (A5), 515−526.

(22) Kolodziej, A.; Krajewski, W.; Dubis, A. Alternative solution for strongly exothermic catalytic reactions: a new metal-structured catalyst carrier. *Catal. Today* **2001**, *69*, 115−120.

(23) de Brito, M. H., von Stockar, U.; Bangerter, A. M.; Bomio, P.; Laso, M. Effective Mass-Transfer Area in a Pilot Plant Column Equipped with Structured Packings and with Ceramic Rings. *Ind. Eng. Chem. Res.* **1994**, *33*, 647−656.

(24) www.sulzerchemtech.com.

(25) Schildhauer, T. J. Untersuchungen zur Verbesserung des Wärmeübergangs in katalytischen Festbettreaktoren für Energiespeicheranwendungen, Ph.D. Thesis No 14301, ETH, Zürich, Switzerland, 2001 (http://e-collection.ethbib.ethz.ch/ecol-pool/diss/fulltext/eth14301.pdf).

(26) Niranjan, K.; Pangarkar, V. G. Hydrodynamic and mass transfer characteristics of polyprolyene wire gauze packings. *Chem. Eng. J.* **1983**, *27*, 49−57.

(27) www.ergaerospace.com.

(28) www.porvair.com.

(29) Calis, H. P. A.; Nijenhuis, J.; Paikert, B. C.; Dautzenberg, F. M.; van den Bleek, C. M. CFD Modelling and Experimental Validation of Pressure Drop and Flow Profile in a Novel Structured Catalytic Reactor Packing. *Chem. Eng. Sci.* **2001**, *56*, 1713−1720.

(30) Maiti, R.; Khanna, R.; Nigam, K. D. P. Hysteresis in trickle-bed reactors: A Review. *Ind. Eng. Chem. Res.* **2006**, *45*, 5185−5198.

(31) Attou, A.; Boyer, C. Hydrodynamics of gas-liquid-solid trickle-bed reactors: A critical review [Revue des aspects hydrodynamiques des reacteurs catalytiques gaz−liquide−solide a lit fixe arose.] *Rev. Inst. Fr. Petrol.* **1999**, *54*, 29−66.

(32) Maiti, R. N.; Sen, P. K.; Nigam, K. D. P. Trickle-bed reactors: Liquid distribution and flow texture. *Rev. Chem. Eng.* **2004**, *20*, 57−109.

(33) Boelhouwer, J. G.; Piepers, H. W.; Drinkenburg, A. A. H. Nature and characteristics of pulsing flow in trickle-bed reactors. *Chem. Eng. Sci.* **2002**, *57*, 4865−4876.

(34) Al-Dahhan, M. H.; Khadilkar, M. R.; Wu, Y.; Dudukovic, M. P. Prediction of pressure drop and liquid hold-up in high-pressure trickle-bed reactors. *Ind. Eng. Chem. Res.* **1998**, *37*, 793−798.

(35) Heibel, A. K.; Vergeldt, F. J.; van As, H.; Boger, T.; Kapteijn, F.; Moulijn, J. A. Gas and Liquid Distribution in the Monolith Film Flow Reactor. *AIChE J.* **2003**, *41*, 3007−3017.

(36) Heiszwolf, J. J.; Kreutzer, M. T.; van den Eijnden, M. G.; Kapteijn, F.; Moulijn, J. A. Gas-Liquid Mass Transfer of Aqueous Taylor Flow in Monoliths. *Catal. Today* **2001**, *69*, 51−55.

(37) Andersson, B.; Irandoust, S.; Cybulski, A. Modeling of monolith reactors in three phase processes. In *Structured Catalysts and Reactors*; Cybulski, A., Moulijn, J. A., Eds.; Marcel Dekker: New York, 1996.

(38) Stichlmair, J.; Bravo, J. L.; Fair, J. R. General Model for Prediction of Pressure Drop and Capacity of Countercurrent Gas/Liquid Packed Columns. *Gas Sep. Purif.* **1989**, *3*, 19−28.

(39) Al-Dahhan, M.; Highfill, W.; Friedman, M. Assessment of the effects of high-pressure operation on the liquid-solid mass-transfer coefficient in trickle-bed reactors. *Ind. Eng. Chem. Res.* **1997**, *36*, 4421−4426.

(40) Kushalkar, K. B.; Pangarkar, V. G. Liquid hold-up and dispersion in packed columns. *Chem. Eng. Sci.* **1990**, *45*, 759−763.

(41) Macias-Salinas, R.; Fair, J. R. Axial mixing effects in packed gas-liquid contactors. *Ind. Eng. Chem. Res.* **2002**, *41*, 3429−3435.

(42) Yawalkar, A. A.; Sood, R.; Kreutzer, M. T.; Kapteijn, F.; Moulijn, J. A. Axial mixing in monolith reactors: Effect of channel size. *Ind. Eng. Chem. Res.* **2005**, *44*, 2046−2057.

(43) Levenspiel, O. *Chemical Reaction Engineering*; John Wiley and Sons: New York, 1999.

(44) Shah, Y. T.; Stiegel, G. J.; Sharma, M. M. Backmixing in gas-liquid reactors. *AIChE J.* **1978**, *24*, 369.

(45) Berglin, C. T.; Herrman, W. A method in the production of hydrogen peroxide. European Patent 102,934 A2, 1984.

(46) Kreutzer, M. T.; Kapteijn, F.; Moulijn, J. A.; Heiszwolf, J. J. Multiphase monolith reactors: chemical reaction engineering of segmented flow in microchannels. *Chem. Eng. Sci.* **2005**, *60*, 5895−5916.

(47) Lehner, P.; Turek, T.; Roy, S.; Bauer, T.; Al-Dahhan, M. Monoliths as multiphase reactors-A review. *AIChE J.* **2004**, *50*, 2918.

(48) Lebens, P. J. M.; Stork, M. M.; Kapteijn, F.; Sie, S. T.; Moulijn, J. A. Hydrodynamics and Mass Transfer Issues in a Counter-current Gas−Liquid Internally Finned Monolith Reactor. *Chem. Eng. Sci.* **1999**, *54*, 2381−2389.

(49) Nijhuis, T. A.; Beers, A. E. W.; Vergunst, T.; Hoek, I.; Kapteijn, F.; Moulijn, J. A. Preparation of monolithic catalysts. *Catal. Rev. Sci. Eng.* **2001**, *43*, 345−380.

(50) Tronconi, E.; Groppi, G. A Study on the Thermal Behaviour of Structured Plate-Type Catalysts with Metallic Supports for Gas/Solid Exothermic Reactions. *Chem. Eng. Sci.* **2000**, *55*, 6021−6036.

(51) Vergunst, T.; Linders, M. J. G.; Kapteijn, F.; Moulijn, J. A. Carbon-based Monolith Structures. *Cat. Rev.* **2001**, *43*, 291−314.

(52) Schildhauer, T. J.; Kapteijn, F.; Moulijn, J. A. Stacking of Film-Flow Monoliths for Improved Performance in Reactive Stripping. *Ind. Eng. Chem. Res.* **2005**, *44*, 9556−9560.

(53) Heibel, A. K.; Lebens, P. J. M. In *Structured Catalysts and Reactors*, 2nd Edition; Cybulski, A., Moulijn, J. A., Ed.; CRC Press: Boca Raton, FL, 2006; pp 479−505.

(54) Lebens, P. J. M. Development and design of a monolith reactor for gas-liquid countercurrent operation. Ph.D. Thesis, Delft University of Technology, Delft, The Netherlands, 1999.

(55) Kreutzer, M. T.; van der Eijnden, M. G.; Kapteijn, F.; Moulijn, J. A.; Heiszwolf, J. J. The Pressure Drop Experiment to Determine Slug Lengths in Multiphase Monoliths. *Catal. Today* **2005**, *105*, 667−672.

(56) Kreutzer, M. T.; Wei, W.; Kapteijn, F.; Moulijn, J. A.; Heiszwolf, J. J. Pressure drop of Taylor flow in capillaries: impact of slug length. *First Int. Conf. Microchannels Minichannels* **2003**, (Apr. 21−23), 1−8.

(57) Lebens, P. J. M.; Heiszwolf, J. J.; Kapteijn, F.; Sie, S. T.; Moulijn, J. A. Gas-liquid Mass Transfer in an Internally Finned Monolith Operated Countercurrently in the Film Flow Regime. *Chem. Eng. Sci.* **1999**, *54*, 5119−5125.

(58) Heibel, A. K.; Heiszwolf, J. J.; Kapteijn, F.; Moulijn, J. A. Influence of Channel Geometry on Hydrodynamics and Mass Transfer in the Monolith Film Flow Reactor. *Catal. Today* **2001**, *69*, 153−163.

(59) Bercic, G.; Pintar, A. The Role of Gas Bubbles and Liquid Slug Lengths on Mass Transport in the Taylor Flow Through Capillaries. *Chem. Eng. Sci.* **1997**, *52*, 3709−3719.

(60) Grolman, E.; Edvinsson, R. K.; Stankiewicz, A.; Moulijn, J. A. Hydrodynamic Instabilities in Gas−Liquid Monolith Reactors. *Proc. ASME Heat Transfer Div.* **1996**, *3*, 171−178.

(61) Irandoust, S.; Ertle, S.; Andersson, B. Gas-Liquid Mass Transfer in Taylor Flow Through a Capillary. *Can. J. Chem. Eng.* **1992**, *70*, 115−119.

(62) Kreutzer, M. T.; Du, P.; Heiszwolf, J. J.; Kapteijn, F.; Moulijn, J. A. Mass Transfer Characteristics of Three-Phase Monolith Reactors. *Chem. Eng. Sci.* **2001**, *56*, 6015−6023.

(63) Heibel, A. K.; Scheenen, T. W. J.; Heiszwolf, J. J.; van As, H.; Kapteijn, F.; Moulijn, J. A. Gas and Liquid Phase Distribution and their Effect on Reactor Performance in the Monolith Film Flow Reactor. *Chem. Eng. Sci.* **2001**, *56*, 5935−5944.

(64) Groppi, G.; Tronconi, E. Continuous v/s Discrete Models of Non-adiabatic Monolith Catalysts. *AIChE J.* **1996**, *42*, 2382−2387.

(65) Kreutzer, M. T.; Bakker, J. J. W.; Kapteijn, F.; Moulijn, J. A.; Verheijen, P. J. T. Scaling-up multiphase monolith reactors: linking residence time distribution and feed maldistribution. *Ind. Eng. Chem. Res.* **2005**, *44*, 4898−4913.

(66) Patrick, R. H.; Klindera, T.; Crynes, L. L.; Cerro, R. L.; Abraham, M. A. Residence Time Distribution in Three-Phase Monolith Reactor. *AIChE J.* **1995**, *41*, 649−657.

(67) Groppi, G.; Tronconi, E. Honeycomb supports with high thermal conductivity for gas/solid chemical processes. *Catal. Today* **2005**, *105*, 297−304.

(68) Boger, T.; Heibel, A. K. Heat Transfer in Conductive Monolith Structures. *Chem. Eng. Sci.* **2005**, *60*, 1823−1835.

(69) Heiszwolf, J. J.; Engelvaart, L. B.; van der Eijnden, M. G.; Kreutzer, M. T.; Kapteijn, F.; Moulijn, J. A. Hydrodynamic Aspects of the Monolith Loop Reactor. *Chem. Eng. Sci.* **2001**, *56*, 805−812.

(70) De Deugd, R. M.; Chougule, R. B.; Kreutzer, M. T.; Meeuse, F. M.; Grievink, J.; Kapteijn, F.; Moulijn, J. A. Is a Monolith Loop Reactor a Viable Option for Fischer Tropsch Synthesis? *Chem. Eng. Sci.* **2003**, *58*, 583−591.

(71) von Scala, C.; Wehrli, M.; Gaiser, G. Heat Transfer Measurements and Simulation of KATAPAK-M catalyst supports. *Chem. Eng. Sci.* **1999**, *54*, 1375−1381.

(72) Battista, J.; Muzen, A.; Cassanello, M.; Bohm, U. Flow Regime Transitions in Trickle-bed Reactors with Structured Packings. *Can. J. Chem. Eng.* **2003**, *81*, 802−807.

(73) Raynal, L.; Ballaguet, J.-P.; Barrere-Tricca, C. Determination of Mass Transfer Characteristics of Co-current Two-Phase Flow within Structured Packing. *Chem. Eng. Sci.* **2004**, *59*, 5395−5402.

(74) Murrieta, C. R.; Siebert, A. F.; Fair, J. R.; Rocha, J. A. Liquid-Side Mass-Transfer Resistance of Structured Packings. *Ind. Eng. Chem. Res.* **2004**, *43*, 7113−7120.

(75) Shi, M. G.; Mersmann, A. Effective Interfacial Area in Packed Columns. *Ger. Chem. Eng.* **1985**, *8*, 87−96.

(76) Weiland, R. H.; Ahlgren, K. R.; Evans, M. Mass-Transfer Characteristics of Some Structured Packings. *Ind. Eng. Chem. Res.* **1993**, *32*, 1411−1418.

(77) Szulczewska, B.; Zbicinski, I.; Gorak, A. Liquid Flow on Structured Packing: CFD Simulation and Experimental Study. *Chem. Eng. Technol.* **2003**, *26*, 580−584.

(78) Sidi-Boumedine, R.; Raynal, L. Influence of the Viscosity on the Liquid Hold-up in Trickle-Bed reactors with Structured Packings. *Catal. Today* **2005**, *105*, 673−679.

(79) Bravo, J. L.; Rocha, J. A.; Fair, J. R. Mass Transfer in Gauze Packings. *Hydrocarbon Process.* **1985**, *64*, 91−95.

(80) Rocha, J. A.; Bravo, J. L.; Fair, J. R. Distillation Columns Containing Structured Packings: A comprehensive Model for their Performance. 2. mass-transfer model. *Ind. Eng. Chem. Res.* **1996**, *35*, 1660−1667.

(81) de Brito, M. H., von Stockar, U.; Bomio, P. Predicting the liquid phase mass transfer coefficient for the Sulzer structured packing Mellapak. *Inst. Chem. Eng. Symp. Ser.* **1992**, *128*, 137−144.

(82) Brunazzi, E.; Paglianti, A. Liquid-Film Mass-Transfer Coefficient in a Column Equipped with Structured Packings. *Ind. Eng. Chem. Res.* **1997**, *36*, 3792−3799.

(83) Bravo, J. L.; Rocha, J. A.; Fair, J. R. A comprehensive model for the performance of columns containing structured packings. *Inst. Chem. Eng. Symp. Ser.* **1992**, *128*, A439.

(84) Brunazzi, E.; Nardini, G.; Paglianti, A.; Petarca, L. Interfacial area of Mellapak packing: absorption of 1,1,1-Trichloroethane by Genosorb 300. *Chem. Eng. Technol.* **1995**, *18*, 248−255.

(85) Bravo, J. L.; Rocha, J. A.; Fair, J. R. Pressure Drop in Structured Packing. *Hydrocarbon Process.* **1986**, *56*, 45−49.

(86) Rocha, J. A.; Bravo, J. L.; Fair, J. R. Distillation Columns Containing Structured Packings: A comprehensive Model for their Performance. 1. Hydraulic Models. *Ind. Eng. Chem. Res.* **1993**, *32*, 641−651.

(87) Uresti-Melendez, J.; Rocha, J. A. Pressure Drop in Ceramic Structured Packings. *Ind. Eng. Chem. Res.* **1993**, *32*, 2247−2253.

(88) Battista, J.; Bohm, U. Mass Transfer in Trickle-Bed Reactors with Structured Packing *Chem. Eng. Technol.* **2003**, *26*, 1061−1067.

(89) Macias-Salinas, R.; Fair, J. R. Axial mixing effects in packed gas-liquid contactors. *Ind. Eng. Chem. Res.* **2002**, *41*, 3429−3435.

(90) Kołodziej, A.; Jaroszyñski, M.; Schoenmakers, H.; Althaus, K.; Gei*β*ler, E.; Übler, C, Kloeker, M. Dynamic tracer study of column packings for catalytic distillation. *Chem. Eng. Process.* **2005**, *44*, 661−670.

(91) Behrens, M.; Saraber, P. P.; Jansen, H.; Olujic, Z. Performance Characteristics of a Monolith-like Structured Packing. *Chem. Biochem. Eng. Q.* **2001**, *15*, 49−57.

(92) Bragg, L. B. Goodloe Column Packing- A new knit packing material for vapor-liquid contacting operations. *Ind. Eng. Chem.* **1957**, *49*, 1062−1066.

(93) Niranjan, K.; Sawant, S. B.; Joshi, J. B.; Pangarkar, V. G. Countercurrent Absorption using Wire Gauze Packings. *Chem. Eng. Sci.* **1982**, *37*, 367−374.

(94) Patil, V. K.; Sharma, M. M. Packed Tube Columns: Hydrodynamics and Effective Interfacial Area: Pall Rings and Multifilament Wire Gauze Packings. *Can. J. Chem. Eng.* **1981**, *59*, 606−613.

(95) Fourie, J. G.; Du, Plessis, J. P. Pressure drop Modeling in Cellular Metallic Foams. *Chem. Eng. Sci.* **2002**, *57*, 2781−2789.

(96) Richardson, J. T.; Remue, D.; Hung, J. K. Properties of Ceramic Foam Catalyst Supports: mass and heat transfer. *Appl. Catal., A* **2003**, *250*, 319−329.

(97) Montillet, A.; Comiti, J.; Legrand, J. Axial Dispersion in Liquid Flow through Packed Reticulated Metallic Foams and Fixed Beds of Different Structures. *Chem. Eng. J.* **1993**, *52*, 63−71.

(98) Giani, L.; Groppi, G.; Tronconi, E. Heat Transfer Characterization of Metallic Foams. *Ind. Eng. Chem. Res.* **2005**, *44*, 9078−9085.

(99) Giani, L.; Groppi, G.; Tronconi, E. Mass Transfer Characterization of Metallic Foams as Supports for Structured Catalysts. *Ind. Eng. Chem. Res.* **2005**, *44*, 4993−5002.

(100) Stemmet, C. P.; Jongmans, J. N.; van der Schaaf, J.; Kuster, B. F. M.; Schouten, J. C. Hydrodynamics of Gas-Liquid Counter-current flow in Solid Foam Packings. *Chem. Eng. Sci.* **2005**, *60*, 6422−6429.

(101) Stemmet, C. P.; Meeuwse, M.; van der Schaaf, J.; Kuster, B. F. M.; Schouten, J. C. Gas-liquid mass transfer and axial dispersion in solid foam packings. *Chem. Eng. Sci.* **2007**, *62*, 5444−5450.

(102) Richardson, J. T.; Peng, Y.; Remue, D. Properties of Ceramic Foam Catalyst Supports: Pressure Drop. *Appl. Catal., A* **2000**, *204*, 19−32.

(103) Forchheimer, P. H.; Ver. Z. *Dtsch. Ing.* **1901**, *45*, 1781.

(104) Ergun, S. *Ind. Eng. Chem. Eng. Prog.* **1949**, *48*, 89−94.

(105) Stemmet, C. P.; van der Schaaf, J.; Kuster, B. F. M.; Schouten, J. C. Solid Foam Packings For Multiphase Reactors-Modeling of Liquid Holdup and Mass Transfer. *Chem. Eng. Res. Des.* **2006**, *84*, 1134−1141.

(106) Säez, A. E.; Carbonell, R. G. Hydrodynamic Parameters for Gas-Liquid Cocurrent Flow in Packed Beds. *AIChE J.* **1985**, *31*, 52−62.

(107) Klett, J.; Burchell, T. D. High Thermal Conductivity, Mesophase Pitch Derived Carbon Foam. In *Eurocarbon '98: Science and Technology of Carbon*, Strausbourg, France, 1998; French Carbon Group: Strausbourg, France, 1998.

(108) Wang, R.; Mao, Z.; Chen, J. A study of trickling-to-pulsing flow transition in trickle-bed reactors. *Chem. Eng. Commun.* **1994**, *127*, 109−124.

(109) Desmet, G.; De Greef, J.; Verelst, H.; Baron, G. V. Performance limits of isothermal packed bed and perforated monolithic bed reactors operated under laminar flow conditions. I. General optimization analysis. *Chem. Eng. Sci.* **2003**, *58*, 3187−3202.

(110) McGlamery, G. G. Liquid Film Transport Characteristics of Textured Metal Surfaces, Ph.D. Dissertation, The University of Texas at Austin, Austin, TX, 1988.

Received for review January 15, 2008
Accepted February 20, 2008

IE800067R